

Crescentic bedforms in the nearshore region

By G. VITTORI¹, H. E. DE SWART² AND P. BLONDEAUX¹

¹ Istituto di Idraulica, Università di Genova, Via Montallegro 1, 16145, Genova, Italy

² Institute for Marine and Atmospheric Research, Utrecht University, P.O. Box 80.005,
3508 TA Utrecht, The Netherlands

(Received 29 July 1996 and in revised form 7 April 1998)

A wave of small amplitude is considered which approaches a straight beach normally and which is partially reflected at the coastline. By assuming that the local depth is much smaller than the length of the incoming wave, the shallow water equations are used to determine the water motion. The surf zone width is assumed to be small compared to the length of the incoming wave and hence the effect of wave breaking is included only parametrically. The time development of the cohesionless bottom is described by the Exner continuity equation and by an empirical sediment transport rate formula which relates the sediment flux to the steady currents and wave stirring. It is shown that the basic-state solution, which does not depend on the longshore coordinate, may be unstable with respect to longshore bedform perturbations, so that rhythmic topographies form. The instability process is due to a positive feedback mechanism involving the incoming wave, synchronous edge waves and the bedforms. The growth of the bottom perturbations is related to the presence of steady currents caused by the interaction of the incoming wave with synchronous edge waves which in turn are excited by the incoming wave moving over the wavy bed. For natural beaches the model predicts two maxima in the amplification rate: one is related to incoming waves of low frequency, the other to wind waves. Thus two bedforms of different wavelengths can coexist in the nearshore region with longshore spacings of a few hundred and a few tens of metres, respectively. To illustrate the potential validity of the model, its results are compared with field data. The overall agreement is fairly satisfactory.

1. Introduction

The morphology of the beach face and of the sea bed in the nearshore region exhibits a variety of longshore and offshore structures with a broad spectrum of lengthscales ranging from a few centimetres to several kilometres (Allen 1984). Surprisingly often, periodic longshore patterns (beach cusps, giant cusps, crescentic forms, rhythmic topographies) are detected (Komar 1971, 1998). Some of these bedforms appear to be restricted to the beach face (swash cusps) while others extend through the surf zone (surf-zone cusps) and further offshore, sometimes without involving the coastline configuration (crescentic forms and rhythmic topographies: Clos-Arceuduc 1962; Homma & Sonu 1963).

In many studies on the behaviour of bedforms with a rhythmic structure in the longshore direction, it is assumed that they are formed by the combined action of an incoming wave and (alongshore propagating) edge waves. For example in Inman & Guza (1982), Seymour & Aubrey (1985), Dyer (1986) among others, it is shown that

the interaction between an incident monochromatic wave and edge waves produces a periodic pattern in the swash water motion which in turn is supposed to modify the beach face morphology. The main assumption in these studies is that the cusp wavelength is equal to the longshore separation between run-up maxima. This being the case, the cusp wavelength is equal to one-half the wavelength of subharmonic edge waves and is equal to the wavelength of synchronous edge waves (Inman & Guza 1982). Subharmonic and synchronous edge waves are here edge waves characterized by an angular frequency equal to $\omega^*/2$ and ω^* respectively, ω^* being the angular frequency of the incoming wave (hereafter an asterisk denotes dimensional quantities). Although this theory is partly supported by field data, there are also observational studies (Holland & Holman 1996) in which no clear indication of the edge wave mechanism has been detected. A further limitation of these models is that sediment motion is passively driven by water flow and the feedback from the bottom topography to the water motion does not enter the mechanism of cusp formation. Only a further evolution of cusps, which causes nonlinear effects to become relevant, is supposed to lead to a positive coupling between the primary incident wave train and the bedforms. Indeed on a cusped beach, run-up is deflected by horns towards the bays and from there flows seaward as run-off. Incipient topographic depressions on a beach are thus amplified by attracting and accelerating water flow.

Also, the periodic morphologies which are located outside the breaker zone and do not affect the coastline are often related to the presence of edge waves (Holman & Bowen 1982). Indeed the steady drift, generated by the nonlinear self-interaction of edge waves inside the bottom boundary layer, is supposed to cause a net displacement of sediments and is thus found to give rise to bottom patterns similar to those detected in the field. However, in the above model the bed configuration does not enter the mechanism of formation of bottom patterns and the bottom development is again passively driven by the flow field.

An alternative model, developed by Werner & Fink (1993), ascribes shoreface cusp formation to a direct feedback between fluid flow and beach morphology. This seems to be the case because in nature, sea and river bedforms are invariably found to be produced by the instability of the bottom configuration with the secondary flow of the fluid driven by the bed perturbations (Fredsoe 1974; Parker 1976; Richards 1980; Sumer & Bakioglu 1984; Blondeaux & Seminara 1985; Colombini, Seminara & Tubino 1987; Blondeaux 1990; Vittori & Blondeaux 1992; Hulscher, De Swart & De Vriend 1993; Schielen, Doelman & De Swart 1993). The simplified model of Werner & Fink (1993) is based on a numerical algorithm which couples water flow, sediment transport and morphology changes. The main deficiency of this approach, as pointed out by the authors themselves, is the simplified description of the flow in the swash zone. Moreover, this model can only describe the dynamics of the beach face and does not allow predictions about the morphology of the surf zone and of the sea bottom further offshore.

However, topographic surveys of the coastal region (see e.g. Homma & Sonu 1963; Pruszek, Rozynsky & Zeidler 1997) have shown that periodic patterns in the morphology of the nearshore region are present which are of large extent and do not involve the beach face and therefore do not cause any distortion of the straight coastline. An example of such rhythmic bedforms can be observed in figure 1 where the sea bottom morphology observed by Davidson-Arnott & Greenwood (1976) in a region close to the coast is shown. These periodic patterns typically occur in water depths of the order of 10 m, i.e. seaward of the breaker line, and their wavelength is of the order of a few hundreds of metres. The data also indicate that these phenomena

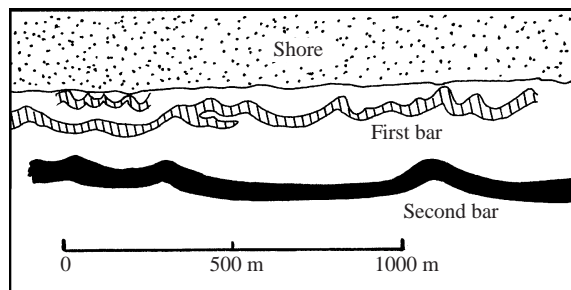


FIGURE 1. Sketch of the longshore bars observed at Kouchibouguac Bay, New Brunswick (Canada) (adapted from Allen (1984) and Davidson-Arnott & Greenwood (1976)).

are quite persistent. Figure 1 shows that other longshore periodic patterns are present in the first bar which however are characterized by shorter wavelengths (of the order of 100 metres and even smaller).

In the present paper the basic idea of Werner & Fink (1993) that rhythmic longshore patterns are due to a feedback between water flow and beach morphology is further developed. It is shown that crescentic forms in the coastal area far away from the swash region and the breaker line can be produced by the time development of small random perturbations both of the sea bottom and of the water motion which interact with a monochromatic wave approaching the beach.

The main objective of the work is to discuss a new morphologic instability mechanism which applies to regions far away from the swash region. Since the dynamics in this region is hardly coupled with that of the coastline and of the beach face, a simplified beach profile is used. This allows an analytical description of the interaction between waves, currents and the erodible bottom. The basic mechanism is that the incoming wave interacts with a small bottom perturbation (periodic in the longshore direction) and produces a synchronous edge wave. This wave subsequently interacts with the incoming wave and leads to the generation of steady currents. The latter induce a net sediment transport with a convergence pattern that is in phase with the bedforms. Hence there is a positive feedback between the water motion and the erodible bottom which gives rise to an exponential growth of both the free surface and the bottom perturbations.

The procedure used in the rest of the paper is the following: in the next section we formulate the problem, while the basic state describing the incoming monochromatic wave partially reflected at the beach is obtained in § 3. In § 4, the time development of a perturbation of the topography coupled with a perturbation of the wave field is studied and the amplitude equations for the most unstable modes are derived. The results are described in § 5. They include the prediction of the frequency of the incoming waves for which rhythmic bedforms are most naturally formed and the values of the longshore spacing of the preferred bottom patterns. These results are compared with field observations to illustrate the potential relevance of the instability mechanism discussed in this paper. A physical interpretation of the instability mechanism is presented in § 6. Finally some conclusions are drawn in § 7.

2. Formulation of the problem

2.1. Reference beach profile

In studies of the coastal region when attention is focused on large-scale phenomena, it is common to introduce a simple idealized beach profile, which can be characterized

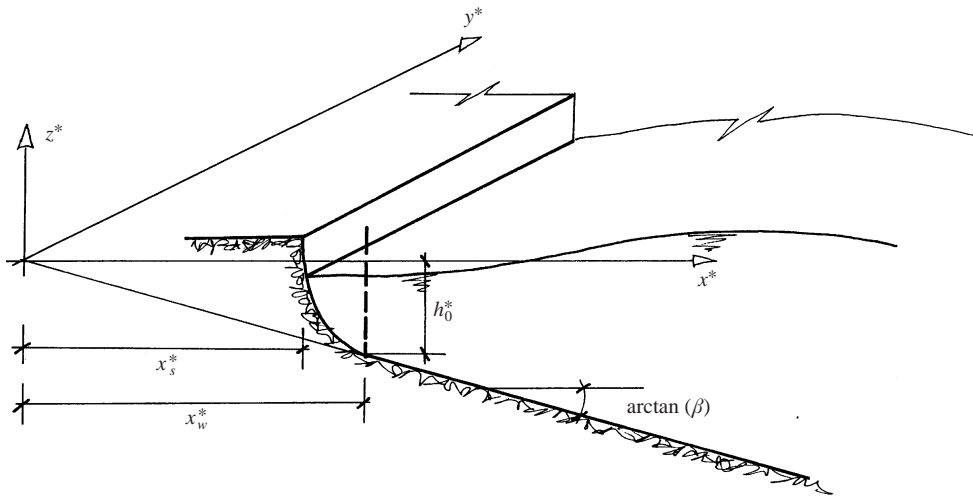


FIGURE 2. Sketch of the problem.

by a few geometrical parameters, and to neglect small-scale details. Field observations show that the bottom slope, averaged over a small spatial extent to filter out small-scale bottom forms, is a decreasing function of the offshore coordinate: close to the coastline the slope is characterized by large values, while far from it the slope is small.

Different approximating laws have been proposed in the past to describe the beach profile, the most widely used being perhaps the 2/3 power law by Bruun (1954) and Dean (1976) describing the mean water depth as function of the offshore coordinate (see also Inman, Elwany & Jenkins 1993). A simpler, idealized yet realistic beach profile is that used in our model and shown in figure 2. It basically consists of two parts: in the outer region ($x^* > x_w^*$, where x^* is the cross-shore coordinate and x_w^* a parameter) the local water depth increases in the seaward direction with a constant slope β , starting from a finite value $h_0^* \equiv \beta x_w^*$ at $x^* = x_w^*$. In the inner region ($x_s^* < x^* < x_w^*$, where x_s^* indicates the position of the shoreline) the beach slope rapidly increases moving towards the beach, resulting in a steep beach at the shoreline. In this paper we will focus our attention on the behaviour of water motion and of the cohesionless bottom in the outer region. Furthermore we will assume that the width of the inner region, i.e. $x_w^* - x_s^*$, is much smaller than the length scale of the wave field. This implies that no detailed study of dynamics within the inner region will be needed and all the phenomena which take place between x_w^* and x_s^* , in particular wave breaking, will be described by means of an appropriate boundary condition at $x^* = x_w^*$. The two independent parameters x_w^* (or h_0^*) and β , which characterize our model beach, can be determined by fitting an observed beach profile. As an example, figure 3 shows beach profiles observed by Howd & Birkemeier (1987) and Lee & Birkemeier (1993) during field measurements carried out at the coast of Duck (North Carolina) and the approximate profile together with the optimum values of x_w^* and β obtained from a least-square fitting. A good description of the long-term cross-shore beach profile is obtained even though small-scale transient phenomena, like storm-generated longshore bars, are neglected. Although there are many natural beaches that are satisfactorily fitted by our simplified geometry, other beach profiles cannot be described by our model and more refined geometries should be used. However, in these cases, it is likely that numerical procedures should be employed to study

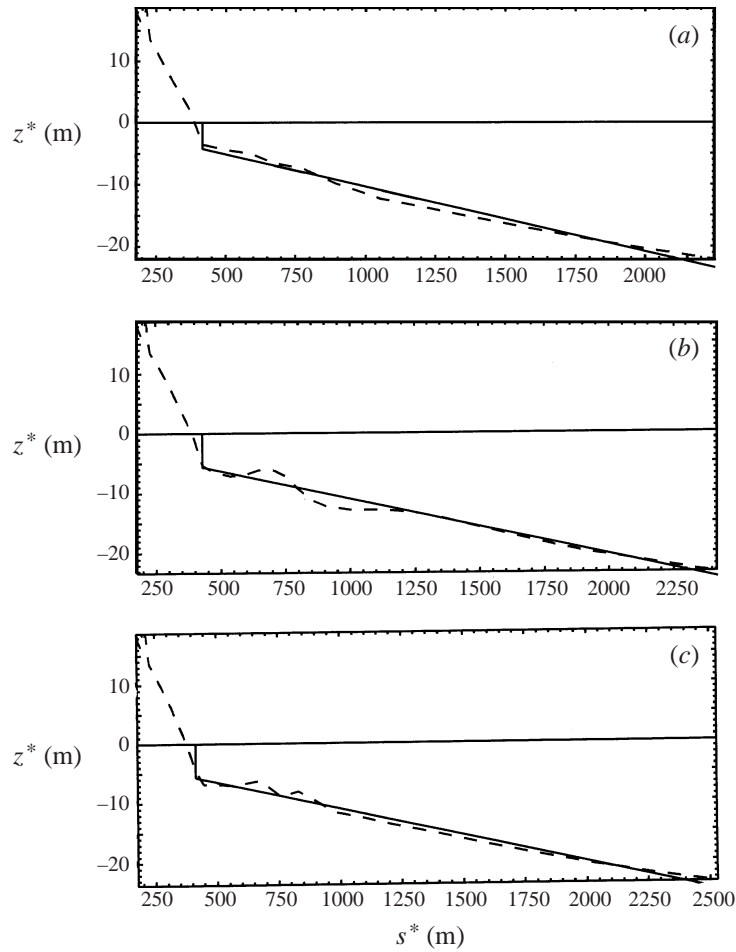


FIGURE 3. Some of the beach profiles observed by Howd & Birkemeijer (1987) and Lee & Birkemeijer (1993) along with our optimized beach geometry. (a) $x_w^* = 381$ m, $\beta = 1.0 \times 10^{-2}$; (b) $x_w^* = 585$ m, $\beta = 9.3 \times 10^{-3}$; (c) $x_w^* = 609$ m, $\beta = 9.1 \times 10^{-3}$.

the time development of the coastal system. Simplified beach profiles are often used by different authors in similar contexts (Guza & Davis 1974; Hino 1974; Bowen & Holman 1989).

2.2. Water motion

By assuming that the horizontal lengthscale of the problem is much larger than the local depth, the water motion in the outer region is described by the shallow water equations. The forcing is due to a prescribed surface gravity wave which approaches the straight beach normally. This wave is assumed to be partially reflected at the coastline and the steady currents generated by nonlinear processes are considered. Moreover, as already implicitly assumed, the amplitude of the incoming wave should be small enough that wave breaking, when it is present, is induced in the inner region only.

It should be remarked that even for very small beach slopes β , the shallow water equations are not uniformly valid and a complete description of the waves would require the matching of the shallow water solution with the solution of the deep

water region. However as discussed by Guza & Davis (1974) and later by Minzoni & Whitham (1977), when attention is focused on wave fields confined to the nearshore region, shallow water equations can be assumed to be uniformly valid.

Let us introduce a Cartesian coordinate system with the x^* - and y^* -axis in the horizontal plane, pointing in the offshore and longshore directions respectively, such that $x^* = 0$ describes the intersection between the still water level and the constant sloping beach profile (see figure 2). If the following non-dimensional variables are defined:

$$(x, y) = (x^*, y^*)\omega^*(g^*h_0^*)^{-1/2}, \quad t = \omega^*t^*, \quad (2.1a)$$

$$(u, v) = (u^*, v^*)(g^*h_0^*)^{-1/2}, \quad \eta = \eta^*/h_0^*, \quad (2.1b)$$

the flow is determined by continuity and momentum equations which are

$$\frac{\partial}{\partial t}[h + \eta] + \frac{\partial}{\partial x}[(h + \eta)u] + \frac{\partial}{\partial y}[(h + \eta)v] = 0, \quad (2.2a)$$

$$\frac{\partial u}{\partial t} + u\frac{\partial u}{\partial x} + v\frac{\partial u}{\partial y} = -\frac{\partial \eta}{\partial x}, \quad \frac{\partial v}{\partial t} + u\frac{\partial v}{\partial x} + v\frac{\partial v}{\partial y} = -\frac{\partial \eta}{\partial y}. \quad (2.2b)$$

In (2.1)–(2.2) t^* is time, u^* and v^* denote the velocity components averaged over the water depth in the x^* - and y^* -directions respectively, η^* is the water surface elevation, ω^* is the angular frequency of the incident wave, ρ^* is fluid density and g^* is the acceleration due to gravity. Finally, h denotes the local depth $h^* = \beta x^*$ divided by h_0^* . It turns out that $h = x/x_w$, where $x_w = \omega^*h_0^{*1/2}/(\beta g^{*1/2})$ is the dimensionless boundary between the inner and outer regions.

Note that in equations (2.2), friction terms are neglected. Moreover, the water motion is considered to be irrotational for both the oscillatory and steady components of the flow. The main motivation for this assumption is that vorticity production takes place close to the bottom and at the coastline and vorticity can be supposed to be confined to a bottom boundary layer and to a region close to the shore.

2.3. Boundary conditions

The flow in the outer region is described by equations (2.2) and forced by the incoming wave partially reflected at the coastline. Hence the solution of (2.2) should be matched with the wave solution in the deep sea which is represented as the superposition of an incoming wave of amplitude a_∞^* and a reflected wave of amplitude $|\hat{K}|a_\infty^*$, where \hat{K} is the complex reflection coefficient of the beach. If it is assumed that the deep water solution is described by linear theory, the matching condition reads

$$\lim_{x \rightarrow \infty} \eta(x, y, t) = \eta_e(x, t) = \lim_{h \rightarrow 0} \frac{1}{2} a_x \left\{ \exp\left(i \int l dx\right) + \hat{K} \exp\left(-i \int l dx\right) \right\} e^{it} + \text{c.c.} \quad (2.3)$$

Here a_x is the local complex wave amplitude, l the cross-shore wavenumber and c.c. denotes a complex conjugate of a complex quantity. Application of the dispersion relation and the energy balance of water waves over a constant sloping bottom yields (Mei 1989, Ch. 3, 11):

$$\lim_{h \rightarrow 0} a_x = \frac{a_\infty^*}{\sqrt{2h_0^*}} (\beta^2 x x_w)^{-1/4}, \quad \lim_{h \rightarrow 0} \int l dx = 2(x_w x)^{1/2} + \varphi, \quad (2.4)$$

with φ an as yet arbitrary phase shift. To obtain the complete solution additional boundary conditions at $x = x_w$ are required, which will be discussed later (see Appendix A).

2.4. Sediment transport and bottom evolution

The time development of the bed configuration is described by the sediment continuity equation, which in dimensionless form reads

$$\frac{\partial h}{\partial t} = \frac{1}{(1-p)} \left[\frac{\partial q_x}{\partial x} + \frac{\partial q_y}{\partial y} \right]. \quad (2.5)$$

In (2.5) $(q_x, q_y) = (q_x^*, q_y^*) / (g^* h_0^{*3})^{1/2}$ denote the x - and y -components of the dimensionless volumetric sediment flux per unit width and p is the porosity of the bottom.

It is generally accepted (cf. Fredsøe & Deigaard 1992) that waves propagating over an erodible fine sand bed generate a sediment suspension with larger sediment concentrations in the near-bed region. When currents are present (either tide-induced, wind-induced or wave-induced as in our case), additional mixing over the water depth occurs, resulting in an increase of the sediment concentration in the upper layers. Measurements in wave flumes show in particular the presence of sediments up to the water surface (Van Rijn 1990, 1993). The basic mechanism of sediment transport in combined current and waves is thus the entrainment of particles by the stirring action of waves and their transport by the current.

If attention is focused on bottom variations which take place on timescales longer than the period of the sea waves, it is reasonable to consider only the sediment transport rate averaged over the wave period. Recently, to quantify the sediments moved by the flow, some approaches have been proposed which are based on a detailed intra-wave analysis in which the transport rate is described within the wave cycle and the time average is carried out afterward. In these approaches the net sediment transport has two contributions: one is proportional to the product of the net horizontal current velocity and the wave-cycle-averaged sediment concentration; the other is induced by the time average of the cross-product of the oscillatory parts of velocity and sediment concentration. Notwithstanding the significant progress that has been made during recent years on the study of the intra-wave sediment transport processes, as pointed out by Ribberink & Al-Salem (1994), our knowledge of these processes is still not complete due to the complex dynamics of sediment particles. Hence in the present work a simpler but more established approach is followed in which the sediment transport rate averaged over the wave period is directly derived from averaged quantities. Following Van Rijn (1990, 1993), the total time-averaged sediment flux due to a steady current superimposed on waves is assumed to be proportional to the depth-averaged current and contains a proportionality factor α which is related to the stirring action of the waves. The stirring coefficient can be described as the time average of some power of the velocity intensity of the waves. Since in our model the basic wave is normally incident, the stirring coefficient is longshore uniform: $\alpha = \alpha(x)$.

Thus we adopt the following parametrization of the dimensionless sediment transport rate:

$$(q_x, q_y) = \tilde{Q} \alpha(x) (\bar{u}, \bar{v}), \quad \alpha = \overline{|u_w|^{b-1}}. \quad (2.6)$$

Here a bar denotes the average over the wave period and u_w is the velocity field of the incoming wave. Furthermore $b > 1$ is an exponent which according to Van Rijn (1993) ranges between 2 and 6 and \tilde{Q} is a dimensionless parameter which depends only on sediment properties.

3. The basic wave field

If the basic wave in the outer region has a characteristic amplitude a^* , which is supposed to be much smaller than h_0^* , the solution can be expanded in terms of the small parameter $a = a^*/h_0^*$:

$$u = aU_1 + O(a^2), \quad \eta = aE_1 + O(a^2), \quad h = x/x_w + O(a^2). \quad (3.1)$$

In the following it will be shown that, because of the matching (2.3) with the deep water solution, the wave amplitude a^* is related to the wave amplitude a_∞^* of the incoming wave far from the coast. In (3.1), because the direction of the incoming wave is orthogonal to the coastline, the v component of velocity is supposed to vanish and all the variables are assumed to be independent of y . Moreover, because U_1 turns out to be a time-periodic function, no bottom changes are induced at $O(a)$.

On substituting (3.1) into (2.2)–(2.3), at $O(a)$ the equations of motion read

$$\frac{\partial E_1}{\partial t} + \frac{\partial}{\partial x} \left[\frac{x}{x_w} U_1 \right] = 0, \quad \frac{\partial U_1}{\partial t} = -\frac{\partial E_1}{\partial x}, \quad (3.2)$$

with the boundary condition

$$\lim_{x \rightarrow \infty} E_1(x, t) = \frac{1}{a} \eta_e(x, t) = \frac{1}{4\pi^{1/2}} (xx_w)^{-1/4} \{ \exp[i(2(xx_w)^{1/2} + \varphi + t)] + \hat{K} \exp[-i(2(xx_w)^{1/2} + \varphi - t)] \} + \text{c.c.} \quad (3.3)$$

where the amplitude a_∞^* of the incoming wave in the deep water region has been related to the amplitude of the wave at the shoreline by

$$a_\infty^* = (\beta/2\pi)^{1/2} a^*. \quad (3.4)$$

The matching condition (3.3), which follows from (2.3)–(2.4), shows that at this order the flow can be assumed time-periodic with dimensionless frequency 1. Then we can write

$$E_1 = \hat{E}_1(x) e^{it} + \text{c.c.}, \quad U_1 = \hat{U}_1(x) e^{it} + \text{c.c.} \quad (3.5)$$

The substitution of (3.1), (3.5) into (2.2) leads to

$$\frac{d}{dx} \left[\frac{x}{x_w} \frac{d\hat{E}_1}{dx} \right] + \hat{E}_1 = 0, \quad (3.6)$$

which allows a solution in terms of Bessel functions (or, equivalently, Hankel functions) which have a well-known asymptotic behaviour for $x \rightarrow \infty$ (see Abramowitz & Stegun 1965). Now if we choose in the matching conditions $\varphi = -\pi/4$, it follows that

$$\hat{E}_1(x) = \frac{1}{2} \{ H_0^{(1)}(2(xx_w)^{1/2}) + \hat{K} H_0^{(2)}(2(xx_w)^{1/2}) \} \quad (3.7a)$$

and

$$\hat{U}_1(x) = \frac{i}{2} (x_w/x)^{1/2} \{ H_1^{(1)}(2(xx_w)^{1/2}) + \hat{K} H_1^{(2)}(2(xx_w)^{1/2}) \}. \quad (3.7b)$$

Here $H_0^{(i)}, H_1^{(i)}$ ($i = 1, 2$) are Hankel functions. Note that the solution found depends on the dimensionless position x_w of the boundary between the outer and inner regions and on the complex reflection coefficient of the beach $\hat{K} = |\hat{K}| e^{i\theta}$. Here θ is the phase shift of the reflected wave with respect to the phase of the incoming wave. A relationship between $x_w, |\hat{K}|$ and θ can be obtained by imposing an appropriate boundary condition at $x = x_w$. For example, let us assume that $x = x_w$ represents

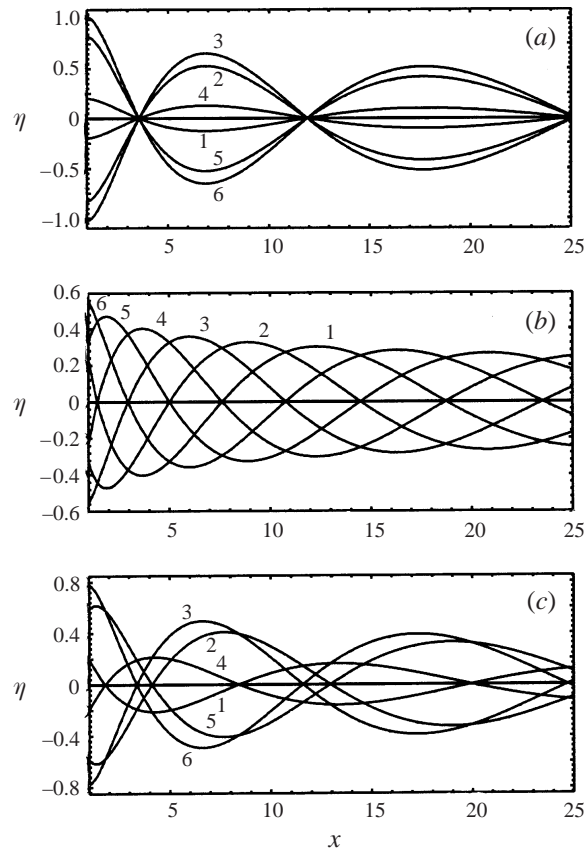


FIGURE 4. Sea surface displacement induced by the incoming wave at different phases during the wave cycle (a) $|\hat{K}| = 1$; (b) $|\hat{K}| = 0$; (c) $|\hat{K}| = 0.5$. The value of θ is determined from Appendix A ($x_w = 1$). Curve 1, $t = 0$; 2, $t = \pi/6$; 3, $t = \pi/3$; 4, $t = \pi/2$; 5, $t = 2\pi/3$; 6, $t = 5\pi/6$.

the position of a vertical wall at which the waves are fully reflected ($|\hat{K}| = 1$). In this so-called 'cliff' case, the instantaneous mass flux must vanish at the wall, yielding at $O(a)$ the boundary condition $\hat{U}_1(x_w) = 0$. From the vanishing of \hat{U}_1 at x_w , the value of θ can be computed once $|\hat{K}|$ is fixed equal to 1. For example for $x_w = 1$, it turns out that θ is about 159° while for $x_w = 10$ the value of θ is 44° . In Appendix A a more general condition is proposed, which is also valid for partially breaking waves if the width of the inner region is small compared to the length of the incoming wave.

In figure 4 the sea surface at different phases during the wave cycle is plotted for an incoming wave which is fully reflected at the coast ($|\hat{K}| = 1$, figure 4a), for an incoming wave which breaks at x_w and is fully absorbed ($|\hat{K}| = 0$, figure 4b) and for an intermediate case ($|\hat{K}| = 0.5$, figure 4c). Here $x_w = 1$ is chosen and boundary condition (A6) has been used to compute the phase shift θ . Because of shoaling, the amplitude of the incoming wave increases as the water depth decreases. If $|\hat{K}| = 1$ (figure 4a) the amplitude of the incoming wave in the deep water region is assumed so small that no breaking occurs and a standing wave is generated. In the second case ($|\hat{K}| = 0$, figure 4b) the amplitude becomes so large that the wave fully breaks and there is no reflection at $x = x_w$. Thus the basic wave is a travelling wave.

4. The longshore perturbations

4.1. The free edge waves

Let us now consider a perturbation of small amplitude ϵ (strictly infinitesimal) superimposed on the basic wave field described in §3. Because of the presence of the small parameter a , it is appropriate to expand the perturbation in terms of a , too:

$$u = aU_1 + O(a^2) + \epsilon[u_0 + au_1 + O(a^2)] + O(\epsilon^2), \quad (4.1a)$$

$$v = \epsilon[v_0 + av_1 + O(a^2)] + O(\epsilon^2), \quad (4.1b)$$

$$\eta = aE_1 + O(a^2) + \epsilon[\eta_0 + a\eta_1 + O(a^2)] + O(\epsilon^2), \quad (4.1c)$$

$$h = \frac{x}{x_w} + O(a^2) + \epsilon[h_0 + ah_1 + O(a^2)] + O(\epsilon^2). \quad (4.1d)$$

First let us discuss the solution of the $O(\epsilon)$ problem. On substituting (4.1) into (2.2)–(2.6), at the leading order of approximation the temporal development and spatial distribution of the perturbation are described by

$$\frac{\partial}{\partial t}[h_0 + \eta_0] + \frac{\partial}{\partial x} \left[\frac{x}{x_w} u_0 \right] + \frac{\partial}{\partial y} \left[\frac{x}{x_w} v_0 \right] = 0, \quad (4.2a)$$

$$\frac{\partial u_0}{\partial t} = -\frac{\partial \eta_0}{\partial x}, \quad (4.2b)$$

$$\frac{\partial v_0}{\partial t} = -\frac{\partial \eta_0}{\partial y}, \quad (4.2c)$$

$$\frac{\partial h_0}{\partial t} = Q \left\{ \frac{\partial}{\partial x} \left[|U_1|^{b-1} \bar{u}_0 \right] + \frac{\partial}{\partial y} \left[|U_1|^{b-1} \bar{v}_0 \right] \right\}, \quad (4.2d)$$

where Q , which turns out to be $\tilde{Q}a^{b-1}/(1-p)$, is a constant much smaller than 1. This because the morphodynamic timescale is much larger than the timescale of the hydrodynamic part of the problem. From a mathematical point of view, the smallness of Q makes it possible to neglect $\partial h_0/\partial t$ in (4.2a).

The boundary condition at $x = x_w$ is discussed in Appendix A and turns out to be

$$u_0 = 0 \quad \text{at} \quad x = x_w. \quad (4.3)$$

Moreover because of condition (2.3) the perturbation should vanish far offshore.

A normal mode approach can be applied and the perturbation will be a superposition of different modes which are periodic in the longshore direction with wavenumber k . Moreover previous works on this subject (Guza & Davis 1974; Blondeaux & Vittori 1995) show that each mode is characterized by an amplitude which depends on a slow timescale $\tau = at$. A preliminary analysis of the problem suggests the following general form for (u_0, v_0, η_0, h_0) :

$$(u_0, v_0, \eta_0) = A(\tau)(\hat{u}_0(x), \hat{v}_0(x), \hat{\eta}_0(x))e^{i(ky + \sigma t)} + \text{c.c.}, \quad (4.4a)$$

$$h_0 = B(\tau)\hat{h}_0(x)e^{iky} + \text{c.c.} \quad (4.4b)$$

By substituting (4.4) into (4.2), it is found that the sediment continuity equation is identically satisfied whatever value of $\hat{h}_0(x)$, while fluid continuity and momentum equations give rise to the following problem:

$$\frac{d}{dx} \left[\frac{x}{x_w} \frac{d\hat{\eta}_0}{dx} \right] - \left(\frac{x}{x_w} k^2 - \sigma^2 \right) \hat{\eta}_0 = 0, \quad (4.5a)$$

$$\hat{u}_0 = \frac{i}{\sigma} \frac{d\hat{\eta}_0}{dx}, \quad \hat{v}_0 = -\frac{k}{\sigma} \hat{\eta}_0. \quad (4.5b)$$

The differential equation (4.5a) admits the bounded non-trivial solution

$$\hat{\eta}_0(x) = e^{-kx} U(d, 1, 2kx), \quad (4.6)$$

where d is equal to $(k - \sigma^2 x_w)/2k$ and U indicates one of the Kummer functions (Abramowitz & Stegun 1965). The part of the solution related to the other Kummer function $M(d, 1, 2kx)$ has been dropped because $\hat{\eta}_0$ should vanish for large values of x . The boundary condition (4.3) provides the dispersion relation

$$d = -\frac{U(d, 1, 2kx_w)}{2U(d+1, 2, 2kx_w)}, \quad (4.7)$$

where the property $(d/dz)U(d, 1, z) = -dU(d+1, 2, z)$ has been used.

Once σ is fixed, relation (4.7) is satisfied by different values d_n ($n = 1, 2, 3, \dots$) of d . They correspond to different modes which are characterized by different wavenumbers in the longshore direction. The cross-shore structure of the free-surface perturbations is described by $\hat{\eta}_0(x)$ which depends on the parameter x_w and on the mode number n . Figure 5 shows that the free-surface perturbations tend to vanish far offshore and are significant in a region the extent of which increases with increasing n . Hence the perturbations turn out to be trapped close to the coast and the term 'edge waves' will be used. The results plotted in figure 5 are obtained for $\sigma = 1$ (synchronous edge waves) and $x_w = 1$ but similar patterns are found for other values of σ and x_w . The longshore wavenumber k of the edge waves is provided by (4.7) when the angular frequency σ and the mode number n are fixed. In figure 6, the dispersion relation (4.7) is plotted for $x_w = 1$ and for the first four modes.

The definition of d shows that, once $|\sigma|$ and k are fixed, two edge waves are possible which travel in opposite directions and which are characterized by opposite real values of σ . Hence the most general linear perturbation of the free surface is described by

$$\eta_0 = \int_0^\infty dk \sum_{n=1}^\infty \{ e^{-kx} U(d_n, 1, 2kx) [A_n^+(k, \tau) e^{i(ky + \sigma_n t)} + A_n^-(k, \tau) e^{i(ky - \sigma_n t)}] + \text{c.c.} \}, \quad (4.8)$$

where $\sigma_n > 0$ indicates the angular frequency of the n -mode and A_n^+ , A_n^- the amplitudes of the components travelling in the negative and positive directions of the y -axis respectively. Equation (4.8) describes the full spectrum of free edge waves for the present geometric configuration of the beach. The constantly sloping beach case with vanishing depth at the coast has been already discussed by Eckart (1951). Note however that in the limit $x_w \rightarrow 0$ our edge wave solution does not converge to Eckart's solution because of the boundary condition (4.3).

4.2. Excitation of synchronous edge waves

So far we have shown that the equations of motion allow both a partially reflected incident wave, forced by the deep water wave condition, and free edge waves described by equation (4.8) plus a bottom perturbation which does not depend on the fast time coordinate t . It can be recognized that the interaction of the edge waves with the incoming wave field results in a correction of the basic perturbation. In particular steady currents will be generated if the edge waves are synchronous, i.e. when they have the same frequency as that of the incident wave.

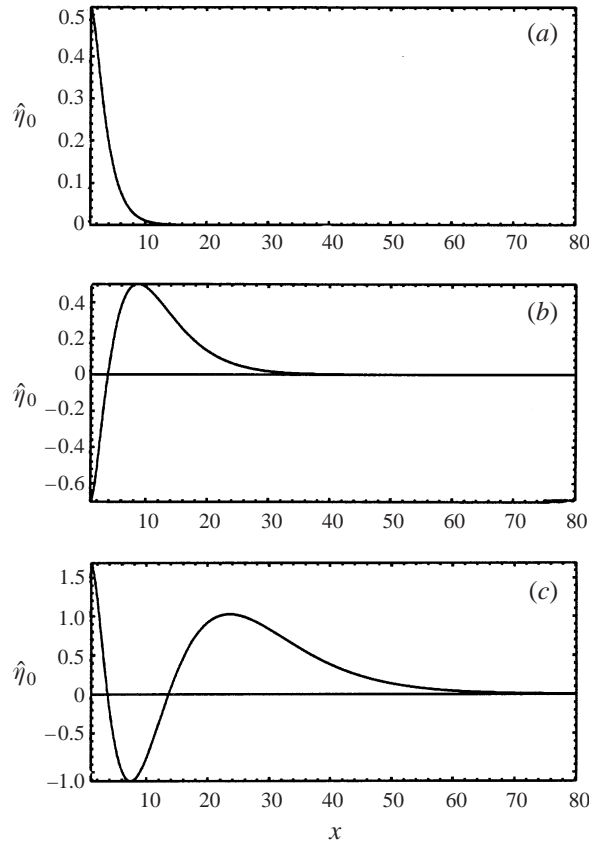


FIGURE 5. Amplitude of sea surface displacement induced by synchronous edge waves ($\sigma = 1, x_w = 1$): (a) $n = 1$; (b) $n = 2$; (c) $n = 3$.

Such interaction is described by the $O(\epsilon a)$ part of the system, which reads

$$\begin{aligned} \frac{\partial}{\partial t}[h_1 + \eta_1] + \frac{\partial}{\partial x} \left[\frac{x}{x_w} u_1 \right] + \frac{\partial}{\partial y} \left[\frac{x}{x_w} v_1 \right] \\ = -\frac{\partial}{\partial x} [h_0 U_1 + E_1 u_0 + \eta_0 U_1] - \frac{\partial}{\partial y} [E_1 v_0] - \frac{\partial h_0}{\partial \tau} - \frac{\partial \eta_0}{\partial \tau}, \end{aligned} \quad (4.9a)$$

$$\frac{\partial u_1}{\partial t} + \frac{\partial \eta_1}{\partial x} = -U_1 \frac{\partial u_0}{\partial x} - u_0 \frac{\partial U_1}{\partial x} - \frac{\partial u_0}{\partial \tau}, \quad (4.9b)$$

$$\frac{\partial v_1}{\partial t} + \frac{\partial \eta_1}{\partial y} = -U_1 \frac{\partial v_0}{\partial y} - \frac{\partial v_0}{\partial \tau}, \quad (4.9c)$$

$$\frac{\partial h_1}{\partial t} = Q \left\{ \frac{\partial}{\partial x} [|U_1|^{b-1} \bar{u}_1] + \frac{\partial}{\partial y} [|U_1|^{b-1} \bar{v}_1] \right\} - \frac{\partial h_0}{\partial \tau}, \quad (4.9d)$$

with boundary conditions

$$u_1 + h_0 U_1 + E_1 u_0 + \eta_0 U_1 = 0 \quad \text{at} \quad x = x_w \quad (4.10)$$

and u_1, v_1, η_1 vanishing for $x \rightarrow \infty$.

In non-resonant cases a solution of the problem for (u_1, v_1, η_1, h_1) forced by the nonlinear interaction of the perturbation with the basic wave field can be found

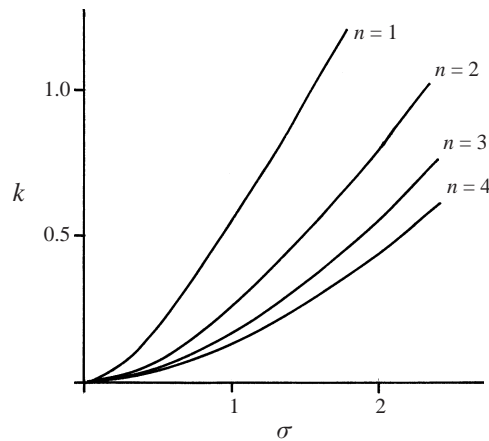


FIGURE 6. Dispersion relation (4.7) for edge waves for the first four modes ($x_w = 1$).

and it gives rise to a slight modification of the original perturbation. Note that the nonlinear forcing terms are proportional to $\exp[(ik_n y)] \exp[\pm i(\sigma_n \pm 1)t]$ and to $\exp[ik_n y] \exp[\pm it]$. If they are characterized by an angular frequency and a longshore wavenumber which correspond to those of a free mode satisfying the dispersion relation (4.7), resonance occurs. As discussed by Guza & Davis (1974), Blondeaux, Vittori & De Swart (1994) and De Swart, Blondeaux & Vittori (1995) many resonating cases exist and in particular resonance is present when the interaction between subharmonic edge waves (frequency $\sigma_n = 1/2$) and the incoming wave is considered. In this case an energy transfer from the basic wave to the edge waves takes place which induces an exponential growth of the edge wave amplitude on the slow timescale τ . Considering the problem (4.9), it can be seen that the presence of the bottom perturbation, which has been neglected so far by other authors, induces the extra forcing term $-\partial[h_0 U_1]/\partial x$ in (4.9a). Since h_0 does not depend on the fast time coordinate t , the forcing term $-\partial[h_0 U_1]/\partial x$ can give rise to a secular growth of η_1 if h_0 has a periodic structure in the longshore direction with wavenumber k equal to that of a synchronous edge wave. Let us focus our attention on this case, i.e. let us consider the solution $\tilde{\eta}_1, \tilde{u}_1, \tilde{v}_1$ of the $O(a\epsilon)$ problem (4.9)–(4.10) which is oscillatory in time with dimensionless frequency equal to 1. This solution is only forced by the first term on the right-hand side of (4.9a), which describes the convergence of the mass flux induced by the incoming wave moving over the bottom perturbation.

The problem can now be recasted in terms of the free surface $\tilde{\eta}_1$ by combining (4.9b) and (4.9c) with continuity equation (4.9a):

$$\frac{\partial^2 \tilde{\eta}_1}{\partial t^2} - \frac{\partial}{\partial x} \left[\frac{x}{x_w} \frac{\partial \tilde{\eta}_1}{\partial x} \right] - \frac{\partial}{\partial y} \left[\frac{x}{x_w} \frac{\partial \tilde{\eta}_1}{\partial y} \right] = -\frac{\partial^2}{\partial x \partial t} [h_0 U_1] - 2 \frac{\partial^2 \tilde{\eta}_0}{\partial t \partial \tau}, \quad (4.11)$$

subject to the boundary condition

$$\frac{\partial \tilde{\eta}_1}{\partial x} = \frac{\partial}{\partial t} (h_0 U_1) \quad \text{at} \quad x = x_w \quad (4.12)$$

and to the constraint of vanishing far from the coast. In deriving (4.12) the fact that the cross-shore velocity component of the free edge wave vanishes at $x = x_w$ has been used. Here $\tilde{\eta}_0$ represents the free surface of synchronous edge waves which, according

to equation (4.8), can be written as

$$\tilde{\eta}_0 = \sum_{n=1}^{\infty} e^{-k_n x} U(d_n, 1, 2k_n x) [A_n^+ e^{it} + A_n^- e^{-it}] e^{ik_n y} + \text{c.c.}, \quad (4.13)$$

with k_n the solution of dispersion relation (4.7) for edge waves characterized by $\sigma = 1$.

Now equations (4.11)–(4.12) describe the dynamics of free synchronous edge waves which are resonantly driven by the forcing terms on the right-hand sides. The latter are due to the interaction between the incoming wave and the bottom perturbation. In order to prevent the solution from growing unbounded on the fast timescale, a solvability condition must be imposed. This is a standard procedure when analysing this type of inhomogeneous differential equations. The condition can be derived by multiplication of (4.11) by a free synchronous edge wave, as given in (4.13) for a fixed n , and averaging the result over the spatial domain and over time. Using partial integration and the boundary conditions (4.3) and (4.12), the following amplitude equations are obtained:

$$\frac{dA^+}{d\tau} = \gamma_1^+ B^+ + \gamma_2^+ B^-, \quad \frac{dA^-}{d\tau} = \gamma_1^- B^+ + \gamma_2^- B^-, \quad (4.14)$$

where $\gamma_1^\pm, \gamma_2^\pm$ are coupling coefficients. It appears that

$$\gamma_1^\pm = \pm i \left\{ \int_{x_w}^{\infty} \left[\hat{h}_0^\pm \left(\frac{d\hat{E}_1}{dx} \right)^\pm \frac{d\hat{\eta}_0}{dx} \right] dx \right\} / \left\{ 2 \int_{x_w}^{\infty} (\hat{\eta})_0^2 dx \right\} \quad (4.15)$$

and the expressions for γ_2^\pm are similar, except that \hat{h}_0^+ should be replaced by \hat{h}_0^- . The mode number n is assumed to be fixed and hence the index n has been dropped. Furthermore B^+, B^- and \hat{h}_0^+, \hat{h}_0^- indicate the amplitude and the cross-shore dependence of the bottom perturbations coupled with A^+ and A^- respectively. Finally, $(d\hat{E}_1/dx)^+$ is $d\hat{E}_1/dx$ while $(d\hat{E}_1/dx)^-$ is the complex conjugate of $d\hat{E}_1/dx$ and $\hat{\eta}_0$ describes the cross-shore structure of the synchronous edge wave, i.e. it is equal to $\hat{\eta}_0(x)$ for $\sigma = 1$. Equations (4.14) relate the growth of the amplitudes A^\pm of synchronous edge waves to the amplitudes of the bottom perturbations.

4.3. The forcing of steady currents

A further link between A^\pm and B^\pm is found by considering the bottom time development forced by the solution of the steady part of the $O(\epsilon a)$ flow problem. This is because the interaction of synchronous edge waves with the incoming wave will generate steady currents, which cause the movement of sediment and thereby result in the formation of bedforms. The equations for the steady currents are obtained from (4.9)–(4.10) by time averaging. If $O(Q)$ contributions are neglected, the result is

$$\frac{\partial}{\partial x} \left[\frac{x}{x_w} \bar{u}_1 \right] + \frac{\partial}{\partial y} \left[\frac{x}{x_w} \bar{v}_1 \right] = -\frac{\partial}{\partial x} \overline{[E_1 u_0 + \eta_0 U_1]} - \frac{\partial}{\partial y} [E_1 v_0], \quad (4.16a)$$

$$\frac{\partial \bar{\eta}_1}{\partial x} = -\overline{\left[U_1 \frac{\partial u_0}{\partial x} + u_0 \frac{\partial U_1}{\partial x} \right]}, \quad \frac{\partial \bar{\eta}_1}{\partial y} = -\overline{U_1 \frac{\partial v_0}{\partial x}}. \quad (4.16b,c)$$

Equation (4.16a) can be combined with the condition $\partial \bar{u}_1 / \partial y = \partial \bar{v}_1 / \partial x$, which follows from the irrotational assumption. A single equation for the longshore component of

the steady velocity is thus obtained:

$$\frac{\partial}{\partial x} \left[\frac{x}{x_w} \frac{\partial \bar{v}_1}{\partial x} \right] + \frac{\partial}{\partial y} \left[\frac{x}{x_w} \frac{\partial \bar{v}_1}{\partial y} \right] = -\frac{\partial^2}{\partial y \partial x} [\overline{E_1 u_0 + \eta_0 U_1}] - \frac{\partial^2}{\partial y^2} [\overline{E_1 v_0}]. \quad (4.17)$$

Equations (4.16)–(4.17) admit solutions of the form

$$(\bar{\eta}_1, \bar{u}_1, \bar{v}_1) = (\hat{\eta}_1, \hat{u}_1, \hat{v}_1) e^{iky} + \text{c.c.}, \quad (4.18)$$

yielding the differential equation

$$\frac{d}{dX} \left[X \frac{d\hat{v}_1}{dX} \right] - X \hat{v}_1 = F^+(x) A^+ + F^-(x) A^-, \quad (4.19)$$

where $X = kx$. Equation (4.19) is subject to the boundary conditions

$$\lim_{X \rightarrow \infty} \hat{v}_1 = 0, \quad \frac{d\hat{v}_1}{dX} = G^+ A^+ + G^- A^- \quad \text{at} \quad X = X_w. \quad (4.20)$$

The expressions for F^\pm and G^\pm are given in Appendix B, where the solution for the steady currents is also derived in terms of modified Bessel functions. It is found that

$$\hat{u}_1 = A^+ u_1^+ + A^- u_1^-, \quad \hat{v}_1 = A^+ v_1^+ + A^- v_1^-. \quad (4.21)$$

4.4. The bottom growth

Next we consider the sediment continuity equation (4.9d). In order to avoid h_1 growing on the fast timescale t , it is necessary that the right-hand side of this equation vanishes. Fixing the mode number, upon substitution of the expression (4.4b) for the bottom perturbation and equations (4.18) and (4.21) for the $O(a\epsilon)$ steady solutions, equation (4.9d) reads

$$\frac{dB^\pm}{d\tau} \hat{h}_0^\pm = Q \left\{ \frac{d}{dx} [|\overline{U_1}|^{b-1} u_1^\pm] + ik |\overline{U_1}|^{b-1} v_1^\pm \right\} A^\pm, \quad (4.22)$$

where we have written $B \hat{h}_0 = B^+ \hat{h}_0^+ + B^- \hat{h}_0^-$.

Now let us focus on the functions \hat{h}_0^\pm which are associated with the steady current solutions u_1^\pm, v_1^\pm . They become

$$\hat{h}_0^\pm(x) = \frac{d}{dx} [|\overline{U_1}|^{b-1} u_1^\pm] + ik |\overline{U_1}|^{b-1} v_1^\pm, \quad (4.23)$$

whereas equation (4.22) implies that

$$\frac{dB^+}{d\tau} = Q A^+, \quad \frac{dB^-}{d\tau} = Q A^-. \quad (4.24)$$

Once $\hat{h}_0^\pm(x)$ are known, the values of γ_1^\pm and γ_2^\pm which appear in (4.15) can be evaluated, thereby closing the problem.

4.5. Analysis of the amplitude equations

If equations (4.14) are combined with equations (4.24), two coupled amplitude equations are obtained which describe the time development of the bottom perturbations:

$$\frac{d^2 B^+}{d\tau^2} = Q [\gamma_1^+ B^+ + \gamma_2^+ B^-], \quad \frac{d^2 B^-}{d\tau^2} = Q [\gamma_1^- B^+ + \gamma_2^- B^-]. \quad (4.25)$$

The solutions of (4.25) are of exponential type with four different roots:

$$B^\pm \sim \exp(\Omega\tau), \quad \Omega = \pm Q^{1/2} \Gamma_1, \quad \Omega = \pm Q^{1/2} \Gamma_2 \quad (4.26)$$

and

$$\Gamma_{1,2} = \left(\frac{(\gamma_1^+ + \gamma_2^-) \pm ((\gamma_1^+ + \gamma_2^-)^2 + 4(\gamma_2^+ \gamma_1^- - \gamma_2^- \gamma_1^+))^{1/2}}{2} \right)^{1/2}. \quad (4.27)$$

Taking into account that γ_2^+ and γ_2^- are the complex conjugates of γ_1^- and γ_1^+ respectively, (4.27) can be recasted in the form

$$\Gamma_{1,2} = (\text{Re}(\gamma_1^+) \pm ((\text{Re}(\gamma_1^+))^2 + |\gamma_1^-|^2 - |\gamma_1^+|^2)^{1/2})^{1/2}. \quad (4.28)$$

It thus follows that the bottom perturbations will grow exponentially in time if either $\text{Re}(\Gamma_1)$ or $\text{Re}(\Gamma_2)$ are non-vanishing, where Re refers to the real part. In that case there is a positive feedback between the water motion and the erodible bottom, hence a morphodynamic instability. First, equations (4.14) and (4.24) show that the amplitude of the synchronous edge wave becomes much larger than that of the bottom. Secondly, by substitution of these results into (4.4), it is found that a standing synchronous edge wave will be excited and that the bottom patterns will not migrate. This is a manifestation of the fact that there is no preferred spatial direction in this physical system.

It now remains to be demonstrated that growth rates can indeed be positive. This is the topic of the next section.

5. Discussion of results and comparison with field data

The analysis developed in the previous sections shows that the interaction between a partially breaking incident wave, synchronous edge waves and an erodible bottom may cause the growth of periodic longshore perturbations of the sea bed. Such bottom patterns correspond to solutions of the amplitude equations (4.25) with a positive growth rate, i.e. $\text{Re}(\Omega) > 0$. From equation (4.26) it follows that, if the complex frequencies Γ_1 and Γ_2 are ordered according to the absolute value of their real parts, the condition for instability is $|\text{Re}(\Gamma_1)| \equiv \Gamma_r$ different from zero. The value of Γ_r is controlled by the parameters of the model, i.e. by $x_w, |\hat{K}|, \theta$, the mode number n and the value of the exponent b appearing in the stirring coefficient.

To demonstrate that instability occurs for realistic values of the parameters, contour plots of Γ_r are shown in figure 7 for the first three synchronous edge waves ($n = 1, n = 2$ and $n = 3$). The variables along the horizontal and vertical axes are the reflection coefficient $|\hat{K}|$ and the phase shift θ of the reflected wave, respectively (we recall that $\hat{K} = |\hat{K}|e^{i\theta}$). Furthermore, the dimensionless parameter x_w is fixed equal to 1 and the exponent b in the wave stirring coefficient equals 4, according to the arguments discussed in Van Rijn (1993). The dotted curves in the plots indicate the relation between θ and $|\hat{K}|$ obtained by means of the simple wave model discussed in Appendix A. The main conclusion from these plots is that there is indeed a positive feedback between the bottom and the water motion, resulting in an exponential growth of the bedforms and of the amplitude of the synchronous edge waves. This can also be seen from figure 8, which shows the dependence of the growth rate on the reflection coefficient, computed along the dotted curves in the contour plots of figures 7(a–c). It appears that, at least for $x_w = 1$ and $b = 4$, the largest growth rate occurs for the lowest mode number, which has the smallest wavelength in the longshore direction. In this case the largest amplification rate Γ_z is about 0.0017 and it occurs for $|\hat{K}| \simeq 0.65$ and $\theta \simeq 160.8^\circ$. Moreover, it is noteworthy that neither non-breaking

waves ($|\hat{K}| = 1$) nor fully breaking waves ($|\hat{K}| = 0$) induce bedform growth. Similar results are obtained for different values of x_w .

The physically most preferred conditions for this instability mechanism can be understood as follows. In our linear model incoming random sea waves can be represented by the superposition of an infinitely large number of non-interacting components characterized by different frequencies ω^* and by amplitudes a^* which depend on ω^* . In the dimensionless version of the problem, these wave components are represented by different values of the parameter x_w , which can be interpreted as a dimensionless frequency, and of the dimensionless amplitude a which is a function of x_w . It is therefore interesting, although not conclusive, to look at the maximum value of Γ_r versus x_w for different values of $|\hat{K}|$, by fixing θ according to the simple wave model discussed in Appendix A. Figure 9 shows that the maximum of Γ_r occurs for $x_w \simeq 0.9$ for $|\hat{K}| = 0.9$, i.e. for highly reflected waves. For decreasing values of $|\hat{K}|$, the maximum of Γ_r occurs for larger values of x_w which however remain close to 1. Since for real beaches $(g^* h_0^*)^{1/2} / x_w^*$ ranges between 0.01 and 0.1 s⁻¹, this implies that waves which cause the largest values of Γ_r belong to the class of low-frequency waves.

In order to compute the growth rate of the bedforms we return to the equations (4.26) and (4.27) which show that the amplitude of the fastest growing bottom perturbation behaves like

$$B^\pm \sim \exp(Q^{1/2} \Gamma_1 a \omega^* t^*), \tag{5.1}$$

where the relationship $\tau = a \omega^* t^*$ has been used and a star indicates that a variable is dimensional. The parameter Q is related to the ratio between the hydrodynamical and morphodynamical timescales and it can be written as

$$Q = \frac{\tilde{Q} a^{b-1}}{1-p}. \tag{5.2}$$

Substituting this result in (5.1) and using $\omega^* = x_w (g h_0^*)^{1/2} / x_w^*$, we find

$$B^\pm \sim \exp(a^{(b+1)/2} \tilde{\Omega} \tilde{t}), \quad \tilde{\Omega} = \Gamma_1 x_w, \quad \tilde{t} = t^* \left(\frac{\tilde{Q} g^* h_0^*}{(1-p)(x_w^*)^2} \right)^{1/2}. \tag{5.3}$$

Here \tilde{t} is a new dimensionless time coordinate obtained using a morphodynamic timescale which is constant for given characteristics of the beach. Hence, the most preferred conditions follow from plotting the growth rate versus the dimensionless frequency x_w and looking for the value/values of x_w for which the growth rate attains a maximum. This procedure defines the preferred frequency/frequencies of the incoming wave which triggers the formation of crescentic forms.

The computation of the growth rate thus requires a known dependence of the amplitude a on the dimensionless frequency x_w . In principle this information can be extracted from measured wave spectra which however depend on the site and wave climate. It is interesting to point out that for actual wave spectra, it is likely that the curves of the growth rate versus x_w show at least two maxima. The former is associated with the maximum of $a(x_w)$ attained for values of x_w which are characteristic of wind waves ($x_w \sim 50$). The latter is due to the maximum of $\Gamma_r(x_w)$ which occurs, as shown in figure 9, for $x_w \sim 2$. The presence of two or more maxima and hence of two or more preferred wavelengths for the most unstable crescentic forms is supported by the field observations described by Hom-ma & Sonu (1963) which show the simultaneous presence of crescentic bedforms characterized by wavelengths of order 2000–3000 m,

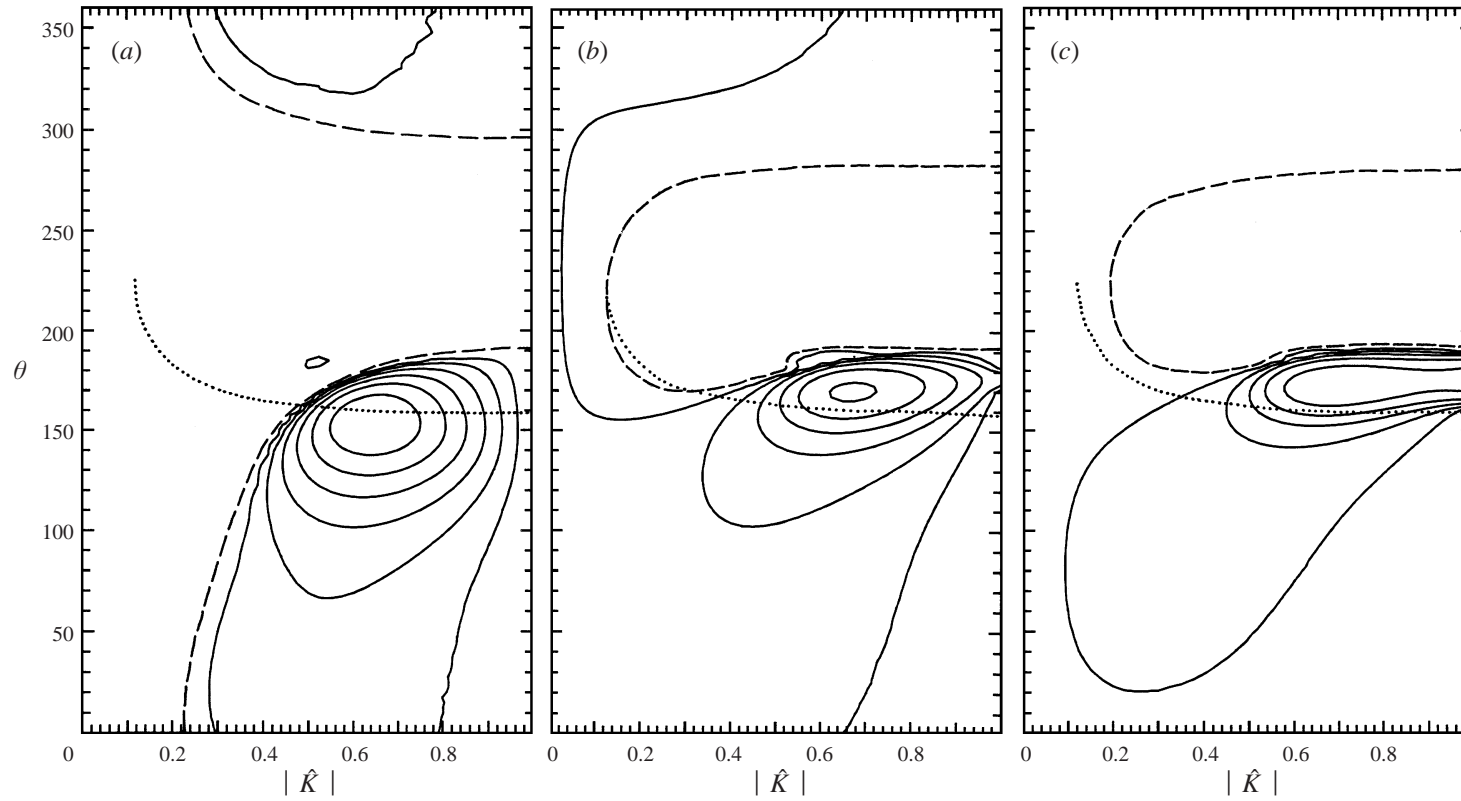


FIGURE 7. The value of Γ_r plotted in the $(|\hat{K}|, \theta)$ -plane ($x_w = 1, b = 4$). Contour line interval equal to 0.0025 (the broken curve represents the $\Gamma_r = 0$ contour). The dotted curves in the plots indicate the relationship between θ and $|\hat{K}|$ as described in Appendix A. (a) $n = 1$; (b) $n = 2$; (c) $n = 3$.

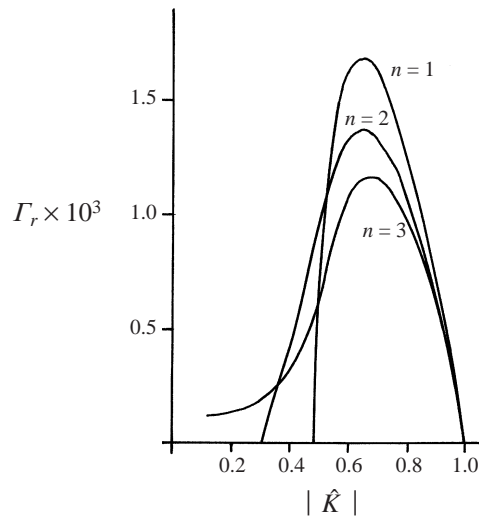


FIGURE 8. Behaviour of Γ_r along the dotted curves of figure 7 ($x_w = 1, b = 4$).

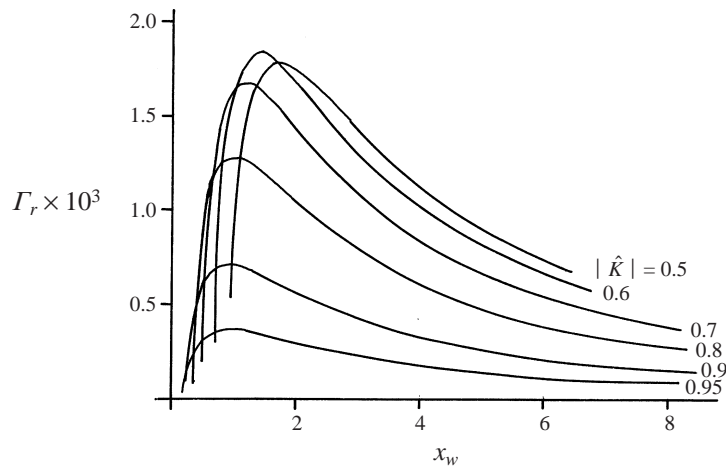


FIGURE 9. Maximum value of Γ_r plotted versus the dimensionless frequency x_w for different values of $|\hat{K}|$ ($n = 1, b = 4$).

200–300 m and 30–60 m (see figure 10 where the small and medium forms clearly appear).

While the value of x_w which gives rise to the first maximum is related to the angular frequency of the most energetic wind wave, the value of x_w which corresponds to the second maximum can be predicted as follows. First, our model setting suggests that we have to consider wave spectra which are measured outside the breaker zone. Second, as already pointed out, x_w -values of order 1 represent low-frequency waves. In this range the wave spectrum is almost white, in other words $a(x_w)$ can be assumed constant. Hence the second maximum corresponds exactly to the maximum of $\tilde{\Omega}$ defined in (5.3).

In figure 11 the growth rate $\tilde{\Omega}$ is shown as a function of x_w for $b = 4, n = 1$ and different values of $|\hat{K}|$. From these results it can be seen that the largest growth rate, and thus the most preferred condition for the instability mechanism, is obtained for

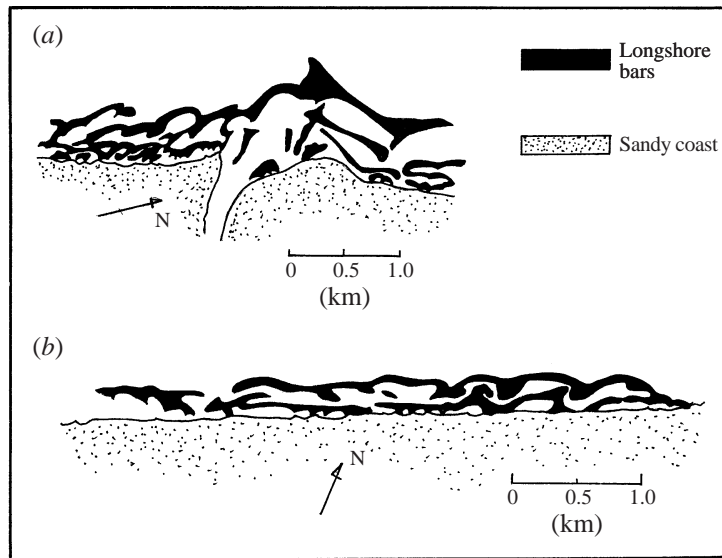


FIGURE 10. Crescentic forms as they appear in the field surveys described in Hom-ma & Sonu (1963) (a) Shin-Shimano site; (b) Niigata west beach. Taken from Hom-ma & Sonu (1963).

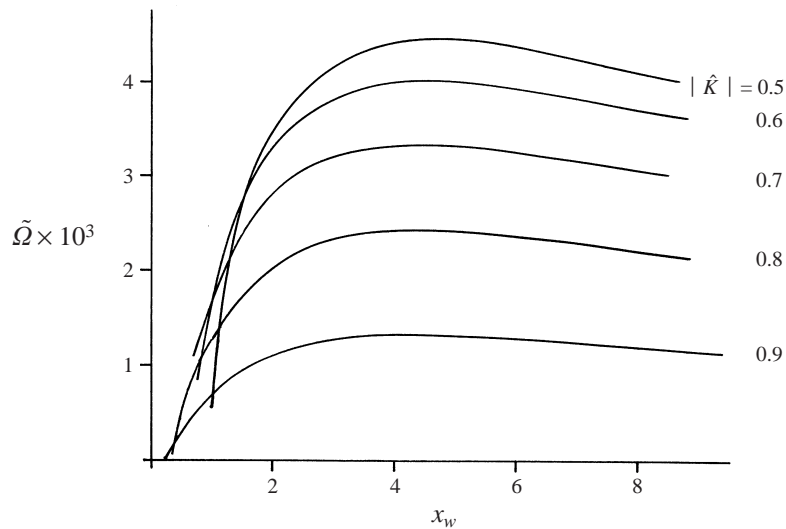


FIGURE 11. Maximum value of the growth rate $\tilde{\Omega}$ plotted versus x_w for different values of $|\hat{K}|$ ($n = 1$, $b = 4$).

$x_w = x_{w,pref} \sim 4.5$ as $|\hat{K}|$ changes from 0.9 to 0.5. However figure 12, where $\tilde{\Omega}$ is plotted versus x_w for different mode numbers and $|\hat{K}| = 0.8$ shows that not always the first mode is the most unstable. When $|\hat{K}|$ is equal to 0.8, the most preferred condition for the instability mechanism is found for $x_w = x_{w,pref}$ equal to about 4.75 and $n = 2$. In this case k is about 0.58. Similar quantitative results are obtained for different values of $|\hat{K}|$.

Let us now consider the spatial structure of the bedforms, of the steady currents

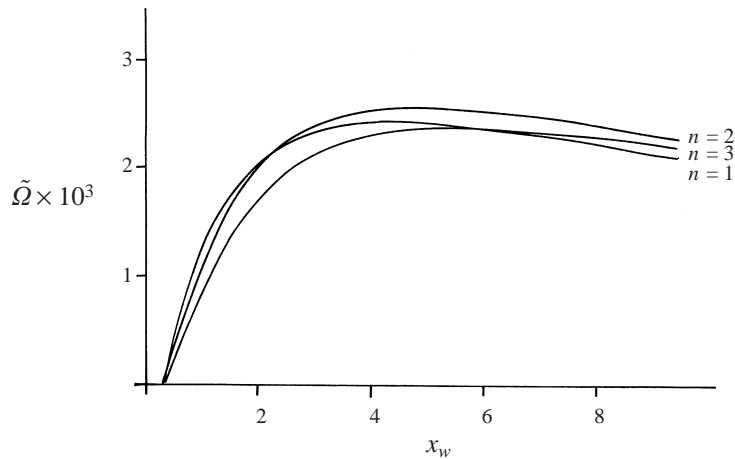


FIGURE 12. Maximum value of the growth rate $\tilde{\Omega}$ plotted versus x_w for different mode numbers n ($|\hat{K}| = 0.8, b = 4$).

and of the steady free-surface displacement for values of the parameters related to these most preferred conditions. A physical interpretation of the results will be given in the next section. In figure 13 contour plots of the bedforms, the steady currents and the steady free-surface displacement are shown for values of x_w and $|\hat{K}|$ such that crescentic forms are generated. The values of the contour lines are arbitrary in this linear model. An overall characteristic of the bottom patterns is that they have a wavelength in the longshore direction which equals that of the synchronous edge wave. Besides, they have two local extrema in the cross-shore direction with a decreasing intensity moving offshore. In accordance with field observations the offshore directed rip currents occur in regions of set-down, whereas an onshore flow can be observed in the regions of set-up. Furthermore, rip currents are found in regions characterized by a sequence of a deep channels close to the coast and a weak bar in the seaward direction.

The value of $x_{w,pref}$, together with its definition, gives a frequency of the incoming wave for which the instability mechanism is most effective. For a beach with given geometrical characteristics (i.e. given values of the dimensional parameters x_w^* and h_0^*), this preferred frequency can be computed together with the spacing of the bedforms and the characteristic timescale of the amplification process. For example by fitting our idealized beach profile to the data described by Homma & Sonu (1963), see § 2.1 and figure 10, it is possible to compute the values of h_0^* and x_w^* . This has been done for the beach profiles observed along the Tokai coast during the years 1956 and 1957 and at the Niigata coast in 1958. Because of the large variability of the bottom topography during storms and mild wave conditions, there is a large uncertainty in the values of h_0^* and x_w^* but it can be stated that h_0^* is approximately 2.5 m and x_w^* is close to 300 m. Assuming that $x_{w,pref} \simeq 4.75$ and $n = 2$ (see figure 12), it turns out that the longshore wavelength of the crescentic bottom forms predicted by our model is about 680 m and the period of the low-frequency waves triggering the morphodynamic instability is around 80 s. This value fairly agrees with the longshore spacings of the medium shoreline bedforms observed during the field surveys at the Tokai and the Niigata coasts. For example in figure 14 the measurements of the bottom depth at the

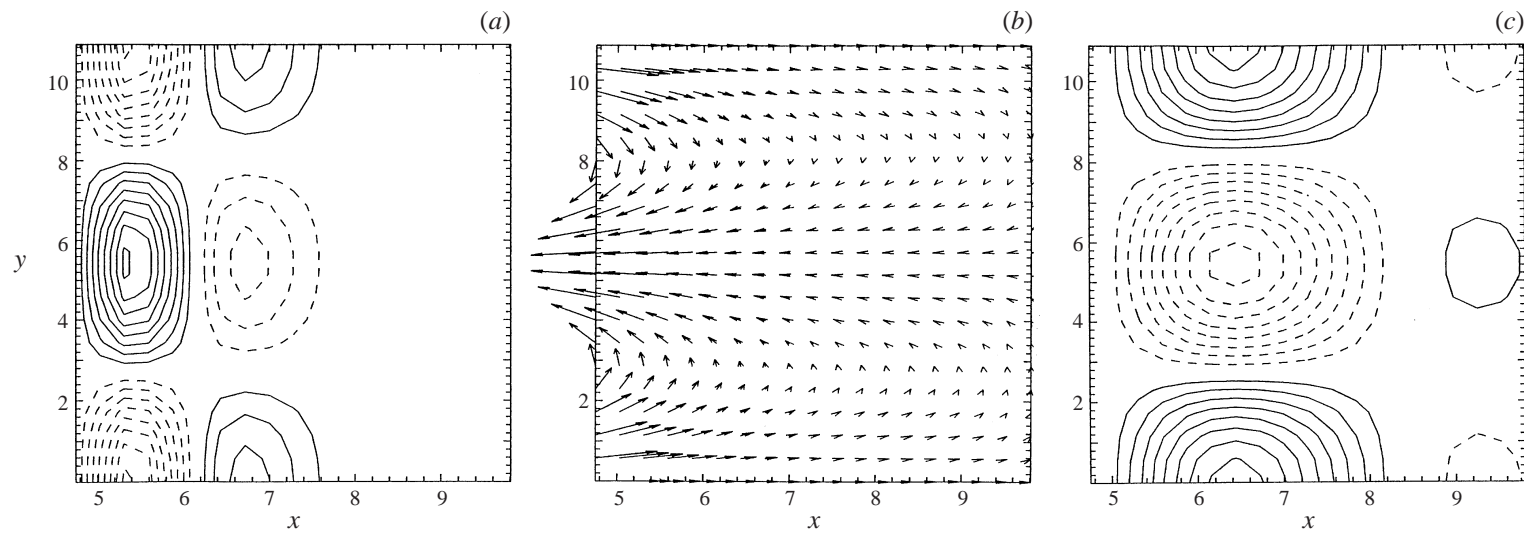


FIGURE 13. Contour plots of (a) the bedforms (---, pools; —, bars), (b) the steady currents and (c) the steady displacement of the free surface (—, set-down; ---, set-up), for $x_w = 4.75$, $n = 2$, $|\hat{K}| = 0.8$ and θ as determined in Appendix A ($b = 4$).

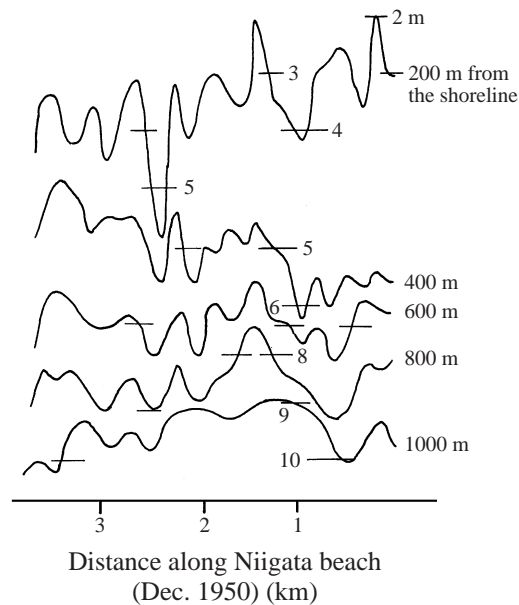


FIGURE 14. Rhythmic undulations of the sea bottom topography of Niigata beach sounded in December 1950 (adapted from Hom-ma & Sonu 1963).

Niigata site clearly show the presence of longshore periodic patterns in the bottom morphology with a wavelength of approximately 500 m.

At the same locations much smaller longshore forms were observed with a spacing ranging between 30 and 60 m (see figure 10). It is likely that these rhythmic patterns are associated with the maximum of the amplification rate due to a peak in the amplitude spectrum $a(x_w)$. Indeed, by assuming that this peak is due to a wave period of about 10 s, it turns out that the predicted wavelength of the induced crescentic forms is approximately 50 m for both sites, which is a value close to the observed wavelengths.

A further comparison with field observations has been performed with the data described by Pruszek *et al.* (1997). Indeed the bottom topography measured at Lubiatawa during summer 1996 also shows the presence of crescentic forms. An analysis of the cross-shore beach profiles suggests that $h_0^* \simeq 2.1$ m and $x_w^* \simeq 370$ m. Then the theory predicts the appearance of longshore periodic forms with a wavelength of 850 m, a value which agrees well with the observed size of the longshore bottom forms (between 600 and 800 m). The smallest crescentic forms which, according to our theory, might be induced by wind waves, were not observed at Lubiatawa. It is likely that the absence of the smallest forms is due to the presence of a system of parallel longshore bars which induces the breaking of wind waves and causes small values of the reflection coefficient $|\hat{K}|$, such that the instability of bottom forms is not triggered.

Finally we consider the sensitivity of our results to the exponent b in the wave stirring factor. This is a relevant point because different values for b are proposed in the literature, usually between 2 and 6 (Van Rijn 1993). In figure 15 growth rates are plotted as functions of the reflection coefficient for mode $n = 1$, $x_w = 1$ and different values of b . Again the phase shift θ has been computed according to the wave model described in Appendix A. Note that for $b \simeq 2.5$ the largest growth rates are found

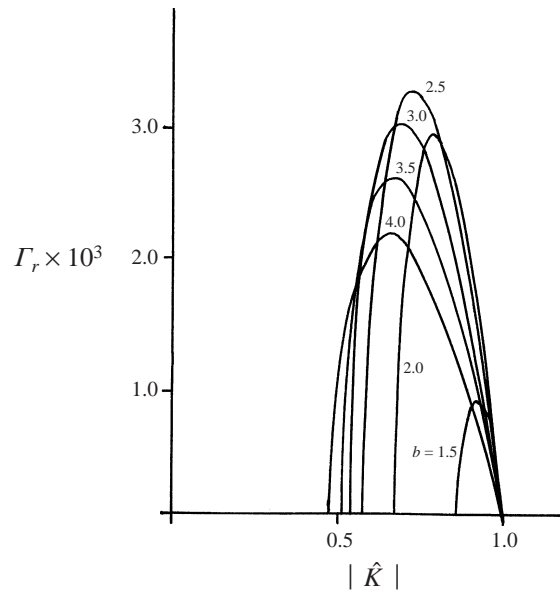


FIGURE 15. Values of Γ_r plotted versus $|\hat{K}|$ for different values of b by considering the first mode, $x_w = 1$ and θ as determined in Appendix A ($b = 4$).

and that for $b = 1$ there are no instabilities. Thus the presence of wave stirring (i.e. $b > 1$) turns out to be essential in order for the instability mechanism to be effective.

6. Physical interpretation

The results found in the previous section can be understood as follows. The interaction between the incoming wave and a specific synchronous edge wave results in both steady mass fluxes and steady momentum fluxes, which have a periodic structure in the longshore direction. These fluxes in turn lead to the occurrence of steady currents and a net steady displacement of the free surface, as can be seen from the averaged continuity and momentum equations (4.16). Since at $x = x_w$ the cross-shore mass flux should vanish (to obey mass conservation in the inner region), the wave-induced steady mass fluxes generate a pattern of alternating seaward- and landward-directed steady velocity components. The intensity of this cross-shore velocity field decreases in the seaward direction because the amplitudes of both the edge wave and the incoming wave become smaller. Since the steady flow is assumed to be irrotational, the longshore variation of the cross-shore velocity component must equal the cross-shore variation of the longshore component. This mechanism gives rise to the spatial patterns of the rip currents observed in figure 13.

As can be seen from the momentum equations (4.16 *b, c*), the steady displacement of the free surface is fully determined by the wave-induced stress. This leads to a rhythmic pattern of set-down and set-up of the free surface in the longshore direction. The observed correlation between the location of a set-down and seaward-directed rip currents is consistent with what is predicted by other models and observed in the field (cf. Bowen 1969; Komar 1998). However, it should be pointed out that our model differs in two respects from the one by Bowen (1969). First, he considered the self-interaction of an incoming wave characterized by a variation of its amplitude in the longshore direction. Instead we compute the direct interaction between an incoming

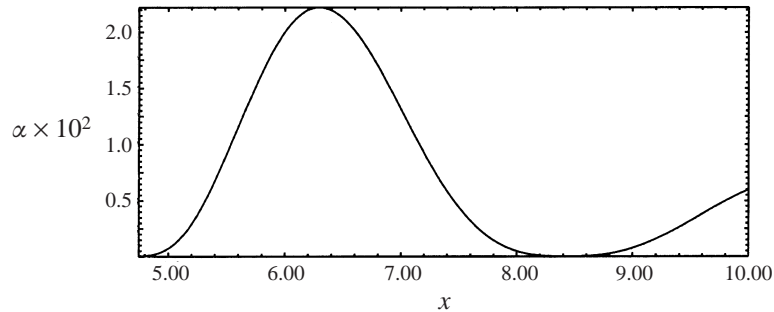


FIGURE 16. Stirring coefficient α as function of the cross-shore coordinate for $x_w = 4.75$, $|\hat{K}| = 0.8$ and θ as determined in Appendix A.

wave (with a uniform amplitude in the longshore direction) and a synchronous edge wave. Secondly, Bowen (1969) used a model in which the only forcing terms are due to wave-induced radiation stresses. Therefore, the rip currents he determined are such that they account for the total depth-integrated steady mass flux, including wave contributions. Instead we start from depth-averaged equations and then split them into the wave- and current-induced parts. Consequently, in our model forcing terms in both the momentum and continuity equations appear.

We now analyse the formation of the bedforms in more detail, as described by equation (4.9d) with $\partial h_1/\partial t = 0$ (see the explanation in §4):

$$\frac{1}{Q} \frac{\partial h_0}{\partial \tau} = \alpha \left\{ \frac{\partial \bar{u}_1}{\partial x} + \frac{\partial \bar{v}_1}{\partial y} \right\} + \frac{d\alpha}{dx} \bar{u}_1. \quad (6.1)$$

Here $\alpha(x)$ is the wave stirring coefficient which only depends on the cross-shore coordinate. The right-hand side of this equation consists of two parts. The first part describes the formation of a shoal (hence decreasing water depths) if the local steady velocity field is convergent and vice versa. The second term is positive if $\bar{u}_1 > 0$ and $d\alpha/dx > 0$ or if $\bar{u}_1 < 0$ and $d\alpha/dx < 0$.

Let us now consider a water column which is moving with the steady velocity field. Because of the increasing water depths in the seaward direction, the column will expand if the flow has an offshore-directed component. In this case the steady cross-shore velocity would be locally convergent because of mass conservation. Hence a bar would tend to appear in a region with an offshore-directed rip current. However, from equation (6.1) it can be immediately seen that a seaward rip current is related to the formation of a pool when the wave stirring coefficient increases in the offshore direction. Thus these two mechanisms can be competitive and the final result depends on the sign of $d\alpha/dx$ as well as on the magnitudes of α and its cross-shore gradient.

In figure 16 the wave stirring coefficient α is plotted as a function of the cross-shore coordinate for values of the parameters equal to those considered in figure 13. It appears that α is small near $x = x_w$; then it increases rapidly to a maximum near $x \simeq 6$. Moving further offshore α is found to decrease up to a value of $x \simeq 8.3$. From figure 13 it appears that, for x roughly between 4.75 and 6.2, the second mechanism dominates over the first one and a pool is generated. For larger values of x the first mechanism is dominant and a bar is formed. This explains the structure of the bedforms as observed in figure 13.

Now according to equation (4.9a) a positive feedback from the bottom to the edge wave motion only occurs if there is a positive time-correlation between the sea level

variations of the synchronous edge wave and $\partial(h_0 U_1)/\partial x$. The latter quantity is the convergence of the perturbed mass flux induced by the incoming waves moving over the bedforms. The results found in the previous section indicate that instability only occurs for moderate reflective conditions. To understand this, we will now demonstrate that the feedback from the bottom to the water motion is negative for both a fully reflected and fully absorbed incoming wave. This analysis will be done for a standing synchronous edge wave, since no preferred direction exist along the y -axis. Here we choose $A^+ = A^- = 1/4$ and from equation (4.13) it follows that the free surface is given as $\eta_0 = \hat{\eta}_0 \cos(k_n y) \cos t$. The cross-shore amplitude function $\hat{\eta}_0$ is defined by equation (4.6) and is positive in the region near $x = x_w$. The corresponding velocity field can be derived from equations (4.2b, c), e.g. the longshore velocity component is $v_0 = k_n \hat{\eta}_0 \sin(k_n y) \sin t$.

Consider now an incoming wave which is fully reflected at a vertical cliff located at $x = x_w$. The free surface and velocity field of the basic wave can be deduced from (3.5)–(3.7) and are

$$E_1 = \tilde{E}_1(x) \cos(t + \theta/2), \quad U_1 = \tilde{U}_1(x) \sin(t + \theta/2), \quad (6.2)$$

where the phase shift θ between the incoming and the reflected wave is such that $\tilde{U}_1(x_w) = 0$. It appears that the cross-shore structures $\tilde{E}_1(x)$ and $\tilde{U}_1(x)$ are both positive in the region $x_w < x < x_n$ where x_n is the location of the first node of the sea level variations. This is a general property of a standing wave.

In order to obtain information on the structure of the bedforms we first consider the steady current pattern. The total steady longshore mass flux, i.e. $(x/x_w)\bar{v}_1 + \overline{E_1 v_0}$, integrated over the cross-section should be constant. This is a consequence of mass conservation and it can be derived by integrating the continuity equation (4.16a) and applying the boundary conditions at $x = x_w$ and far offshore. Moreover the constant is zero, because there is no preferred direction in the system.

Since both the basic wave and the edge wave are standing waves, it follows that the wave-induced steady mass flux $\overline{E_1 v_0}$ will have its largest values at $x = x_w$. Also \bar{v}_1 reaches an extremum at this location, because the flow is irrotational and the cross-shore velocity component \bar{u}_1 is zero at the cliff. In order to obey the mass conservation condition mentioned above it is necessary that the steady mass fluxes $(x/x_w)\bar{v}_1$ and $\overline{E_1 v_0}$ must have different directions near $x = x_w$, hence $\bar{v}_1 \sim -\overline{E_1 v_0}$. The behaviour of the cross-shore steady velocity component is then found by using the fact that the flow is irrotational. This results in the spatial pattern sketched in figure 17.

Now the formation of bedforms is determined by divergences in the sediment transport. From figure 17 it can be seen that at the location of the seaward-directed rip currents, the steady current field is divergent. Moreover, at this location the term $(d\alpha/dx)\bar{u}_1$ is positive, because the wave stirring coefficient increases in the offshore direction. This results in the formation of a pool. Similarly, at the locations where the steady flow is directed onshore a bar will develop.

Using this information it can be shown that in a region near the cliff the perturbed mass flux due to the basic wave moving over the bedforms has a negative time correlation with the cross-shore gradient of the sea surface variation of the synchronous edge wave. Thus, in the case of a fully reflected wave, there is a negative feedback from the bottom to the edge waves. The mathematical translation of this property is that the coupling coefficient γ_1^+ in (4.15) is real and negative and $|\gamma_1^-| = |\gamma_1^+|$ such that in equation (4.28) the quantities $\Gamma_{1,2}$ are zero and imaginary, respectively.

Next, consider an incoming wave which is fully absorbed in the inner region. Again

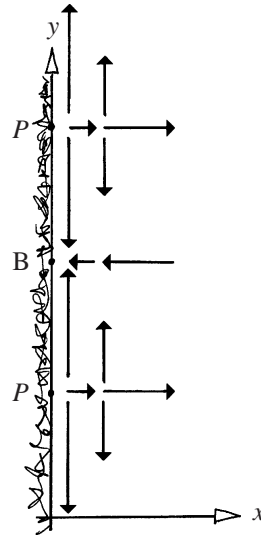


FIGURE 17. Sketch of the steady currents for a vertical cliff located at $x = x_w$ (the incoming wave is a standing wave). The symbols B and P indicate where bars and pool will form.

we will analyse the feedback from the bottom to the edge waves in a region close to the boundary $x = x_w$ where the waves attain their largest amplitudes. The procedure is similar to that of the previous case, hence we first consider the properties of the steady currents. According to boundary condition (4.10), the cross-shore steady flow near the inner region is such that it counterbalances the average cross-shore mass flux induced by the interaction of the incoming wave and the synchronous edge waves. This implies that $\bar{u}_1 \sim -\hat{\eta}_0 \bar{U}_1$. Upon substitution of the known expressions for the incoming wave and the standing synchronous edge wave it follows that $\bar{u}_1 \sim -\hat{\eta}_0 U_{1c} \cos(ky)$. Here the velocity field of the incoming wave has been written as $U_1 = U_{1c} \cos t + U_{1s} \sin t$.

The sediment mass balance (6.1) shows that the structure of the bedforms is related to both the cross-shore steady velocity component and the divergence of the steady flow field. The latter quantity is determined by mass conservation of the water, see equation (4.16a). From this it follows that

$$\frac{\partial \bar{u}_1}{\partial x} + \frac{\partial \bar{v}_1}{\partial y} = \frac{x_w}{x} F - \frac{1}{x} \bar{u}_1, \quad (6.3)$$

where F is the steady mass flux caused by the interaction of the incoming wave and edge waves. Since the wave properties are known this forcing term can be computed and in the region close to $x = x_w$ it turns out to be proportional to $\hat{\eta}_0 U_{1c} \cos(ky)$.

Substitution of these results in equation (6.1) yields that $h_0 \sim \hat{\eta}_0 U_{1c} \cos(ky)$. Here the fact that the stirring coefficient α of a fully absorbed wave decreases in the offshore direction due to shoaling effects has been used. This result shows that $h_0 \sim -\bar{u}_1$, so near the boundary bars will develop at the locations where the rip currents are seaward directed. Furthermore, the perturbed mass flux due to the incoming wave moving over the bedforms has the same time dependence as the standing edge wave and is $U_{1c} h_0 \cos t \sim \hat{\eta}_0 U_{1c}^2 \cos(ky) \cos t$. Close to $x = x_w$ this mass flux, which is proportional to the edge wave amplitude, has a negative time correlation with the cross-shore gradient of the edge wave. Hence a fully breaking incoming wave also does not cause a positive feedback from the bottom to the synchronous edge wave.

Finally we discuss the fact that the preferred conditions for the instability mechanism are found for x_w of order 1. This is a consequence of the fact that the coupling between the incoming wave and a synchronous edge wave is only effective if both waves have approximately the same cross-shore structure. The cross-shore length scale of the incoming wave is determined by the parameter x_w , see equations (3.7), and that of the edge wave by $1/k_n$, where k_n is the wavenumber. Hence preferred conditions are to be expected if $k_n x_w \sim 1$. Since the wavenumber k_n tends to zero for small values of x_w and becomes of order 1 for large values of x_w , the conclusion is that the preferred dimensionless frequency x_w is expected to be of order 1. For a fixed value of x_w the wavenumber k_n decreases with n and thus for higher modes preferred conditions are related to larger values of x_w . This can be clearly seen in figure 9(b).

7. Conclusions

In this paper a new morphodynamic instability mechanism has been discussed. It causes the formation of crescentic bedforms in the nearshore zone of a coastal sea without affecting the beach face and the coastline. As pointed out in the introduction, the existence of such bottom patterns is well documented, see Clos-Arceud (1962), Hom-ma & Sonu (1963) and Pruszek *et al.* (1997). The mechanism consists of two parts which involve hydrodynamic and morphodynamic interactions, respectively. First, the interactions between a normally incident basic wave (which is forced in deep waters and partially reflected at the beach) and synchronous edge wave perturbations force the presence of steady currents with a rhythmical structure in the longshore direction. These currents cause a net transport of sediment and the spatial divergence patterns result in bottom perturbations. Second, the interaction between the forced wave and the bedforms causes perturbed mass fluxes which are in principle able to resonantly force the synchronous edge waves.

This mechanism has been studied for a simple coastal system which consists of two regions. In the so-called outer region the undisturbed bottom is modelled with a constant slope. The profile is assumed to be steeper in the inner region, of which the width is assumed to be small compared to the wavelength of the forced wave. This means that the instability process can be studied in the outer region and the effect of wave breaking can be parametrized by the reflection coefficient $|\hat{K}|$ of the beach and the phase shift θ between the incoming and reflected waves. The value of the latter parameter depends on $|\hat{K}|$ itself and on the beach geometry as has been demonstrated in Appendix A by considering a simple wave breaking model.

It has been shown that a positive feedback from the bottom to the water motion indeed exists for realistic choices of the wave and beach parameters. The linear theory developed in this paper yields an amplification rate for the exponential growth of the amplitudes of the edge waves and bedforms. This growth rate depends on the beach and wave parameters and appears to be positive for moderate reflective conditions: no instabilities are found when the forced wave is fully reflected or fully absorbed in the inner region.

The model analysed in this paper predicts a maximum growth rate in both the low-frequency and high-frequency wave regimes. In the former case (highly reflective conditions) a preferred wave period of the order of 100 s is found, the wavelength of the bedforms in the longshore direction is of the order of 500 m and the e-folding timescale of the growth process is a few months. In the latter case the characteristic wave period is 10 s, the longshore wavelength of the crescentic forms is 50 m and the e-folding timescale is a few days. These predictions have been compared with

data observed at some Japanese and Polish beaches. The agreement turns out to be satisfactory, especially regarding the many simplifying assumptions underlying the present model. A detailed validation of the model results against field data has not been carried out because the model has been designed to illustrate the relevance of a morphodynamic instability to describe certain bedforms, rather than to give a realistic description of all physical processes which appear in the coastal region.

An important limitation of our theory is that it only allows for normally incident waves, whereas waves near a natural beach usually have angle with the coastline. This also holds for the low-frequency waves in the shallow water region due to the directional spreading of the wind waves (Lippman, Holman & Bowen 1997). Another point which deserves further attention is the condition of irrotational flow. In reality there are always sources of vorticity which lead to both vertical and horizontal circulations. The former are caused by bottom friction and they are confined to a thin layer near the bottom if the wave amplitude is much larger than the viscous boundary layer thickness. For low-frequency waves this is a doubtful assumption. Vorticity associated with horizontal circulations is merely generated in the breaker zone and advected by steady currents (such as the undertow and rip currents) towards the outer region.

Also the sediment transport parametrization used is a gross simplification of what occurs in reality. Although it incorporates the effect of wave stirring and subsequent transport by steady currents, it neglects the effects of wave asymmetry. This can only be justified for small-amplitude waves and so the results obtained for high-frequency waves should be interpreted with care. Finally we remark that our model can only be applied to beaches which have a small inner region and for waves which break close to the coast. This is done in order to avoid the necessity of giving a detailed description of a breaking wave. Although certain beaches and wave climates obey this criterion, there are many beaches during storm conditions which cannot be described by our idealized model.

Despite all the limitations discussed above, it is interesting to observe that a simple morphologic model is already able to capture some basic characteristics of bottom and wave patterns in the nearshore zone. These encouraging results are a motivation to extend the present theory and study the effects of nonlinearities. This work will ultimately yield important information on the amplitude and long-term behaviour of the bedforms.

The authors wish to thank Professor H. de Vriend for stimulating them to tackle the problem and for promoting the cooperation between Genova and Utrecht Universities.

This research has been partly supported by EU under contract n. MAS3-CT95-0002 (PACE) in the framework of the Marine Science and Technology Programme (MAST-III), by the Office of Naval Research (O.N.R.) under contract n. N00014-97-1-00709 and by the Ministero dell'Università e della Ricerca Scientifica e Tecnologica.

Appendix A. Mass flux boundary condition at x_w (small width of the inner region)

In §3 a solution for the lowest-order basic wave field has been computed, see (3.5) and (3.7). This solution depends on the dimensionless parameter x_w and on the complex reflection coefficient $\hat{K} = |\hat{K}|e^{i\theta}$, where $|\hat{K}|$ is the ratio between the amplitudes of the reflected and incident waves and θ is their phase shift. A problem is that, although values for x_w and $|\hat{K}|$ can be obtained from field observations, no

result for θ is reported in the literature. This problem can be avoided by specifying an appropriate boundary condition for the instantaneous cross-shore mass flux at $x = x_w$: for given values of x_w and $|\hat{K}|$, this condition will determine the value of θ . A second reason to discuss a mass flux boundary condition at $x = x_w$ is that it is required in §4 to compute the edge wave perturbation.

In this study a simple beach profile is used (see the discussion in §2.1 and figure 2) and the width of the inner region ($x_w^* - x_s^*$ in dimensional units) is assumed to be small compared to the length $((g^* h_0^*)^{1/2} / \omega^*)$ of the incoming wave. In dimensionless units this means that

$$l = (x_w^* - x_s^*) \omega^* / (g^* h_0^*)^{1/2} \ll 1. \quad (\text{A } 1)$$

Moreover, incoming waves are assumed to break inside the inner region. Even though these conditions are only satisfied when the beach close to the coast is very steep and under mild wave conditions, they are imposed because they allow an analytical solution of the problem and help to gain a fundamental understanding about the underlying physics of the phenomenon.

First, let us consider a non-breaking wave, for example a small-amplitude incoming wave which is fully reflected at the coastline (thus $|\hat{K}| = 1$) or a wave propagating in the longshore direction. In this case the instantaneous cross-shore mass flux at $x = x_w$ will be balanced by a storage of mass in the inner region due to time changes of the free surface. Since the width of the inner region is assumed to be small, the free surface will be spatially uniform and the mass balance provides

$$u(h + \eta) = -l \frac{\partial \eta}{\partial t} \quad \text{at } x = x_w \quad (\text{non-breaking waves}). \quad (\text{A } 2)$$

Then because of (A 1), it turns out that

$$u(h + \eta) \approx 0. \quad (\text{A } 3)$$

Hence, for non-breaking waves, the mass storage in the inner region can be neglected. This boundary condition is used in §4 for computing the edge waves.

Next, consider an incoming wave with a significant amplitude which breaks close to the coastline because of the rapid decrease of the water depth in the inner region. In this case the mass stored per unit width in the inner region cannot be neglected because of the strong nonlinear effects related to wave breaking. The cross-shore mass flux is controlled by a turbulent bore propagating into the inner region. A simple model, as sketched in figure 18, yields

$$u^*(h^* + \eta^*) = -c^* \Delta \eta^* \quad \text{at } x^* = x_w^* \quad (\text{breaking waves}), \quad (\text{A } 4)$$

where $c^* = (g^* h^*)^{1/2}$ is the phase speed of the bore and $\Delta \eta^*$ its amplitude. Now let us assume that $\Delta \eta^* = \chi \eta^*$, where χ is an empirical constant which is expected to be of order 1. Substitution in (A 4) yields

$$u(h + \eta) = -\chi \eta \quad \text{at } x = x_w \quad (\text{breaking waves}). \quad (\text{A } 5)$$

It is worth pointing out that, because of (3.7) and (A 5), it turns out that

$$\hat{K} = -\frac{\chi H_0^{(1)}(2x_w) - i H_1^{(1)}(2x_w)}{\chi H_0^{(2)}(2x_w) - i H_1^{(2)}(2x_w)}. \quad (\text{A } 6)$$

If \hat{K} is written as $|\hat{K}| e^{i\theta}$, substitution in (A 6) of a specific choice for $|\hat{K}|$ (in the range $[0, 1]$) yields values for both χ and θ .

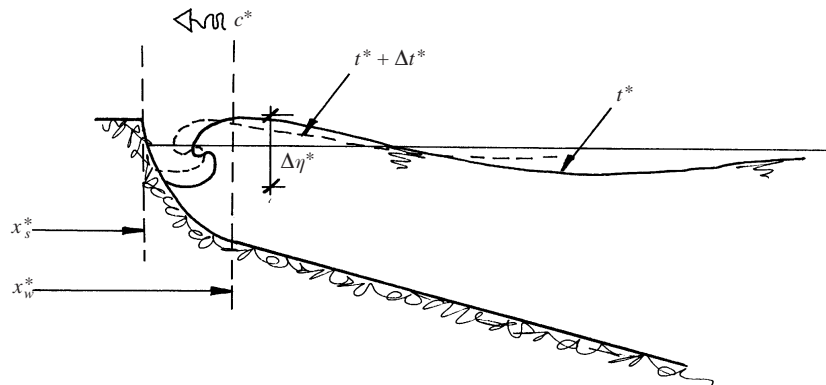


FIGURE 18. Sketch of a turbulent bore propagating in an inner region which has a small width (compared to the distance between successive bores). The mass transported per unit width at $x^* = x_w^*$ in a time interval Δt is stored in the inner region in an area with surface $c^*\Delta t\Delta\eta^*$, where c^* is the bore velocity and $\Delta\eta^*$ its amplitude.

Appendix B. Solutions for the steady currents

In (4.19)–(4.20) the forcing term $F^-(x)$ and constant G^- are

$$F^-(x) = -x_w \left[\hat{E}_1 \frac{d^2 \hat{\eta}_0}{dx^2} - \left(\frac{d^2 \hat{E}_1}{dx^2} + k^2 \hat{E}_1 \right) \hat{\eta}_0 \right], \quad G^- = \hat{\eta}_0 \left(\frac{d\hat{E}_1}{dx} \right)_{x=x_w} \quad (\text{B } 1)$$

whereas F^+ , G^+ are the complex conjugates of $-F^-$ and $-G^-$, respectively.

The solution of (4.19), which has been determined by means of the variation of the parameter method, has one part proportional to A^+ and another proportional to A^- . For the former it is found that

$$v_1^+ = I_0(X) \left[C_1 + \int_{X_w}^X \frac{K_0(\xi) F^+(\xi/k)}{k} d\xi \right] - K_0(X) \left[C_2 + \int_{X_w}^X \frac{I_0(\xi) F^+(\xi/k)}{k} d\xi \right], \quad (\text{B } 2)$$

where $X_w = kx_w$ and I_0, K_0 are the modified Bessel functions. Furthermore the constants C_1, C_2 follow from the boundary conditions (4.20):

$$C_1 = - \int_{X_w}^{\infty} \frac{K_0(\xi/k) F^+(\xi/K)}{k} d\xi, \quad C_2 = - \frac{1}{K_1(X_w)} \{ C_1 I_1(X_w) - G^+ \}. \quad (\text{B } 3)$$

Once v_1^+ is known, the irrotational assumption yields u_1^+ :

$$u_1^+ = - \frac{i}{k} \frac{dv_1^+}{dx}. \quad (\text{B } 4)$$

In a similar way the variables v_1^- and u_1^- can be computed.

REFERENCES

- ABRAMOWITZ, M. & STEGUN, I. A. 1965 *Handbook of Mathematical Functions*. Dover.
 ALLEN, J. R. L. 1984 *Sedimentary Structures*. Elsevier.
 BLONDEAUX, P. 1990 Sand ripples under sea waves. Part 1. Ripple formation. *J. Fluid Mech.* **218**, 1–17.
 BLONDEAUX, P. & SEMINARA, G. 1985 A unified bar-bend theory of river meanders. *J. Fluid Mech.* **157**, 449–470.
 BLONDEAUX, P. & VITTORI, G. 1995 The nonlinear excitation of synchronous edge waves by a monochromatic wave normally approaching a plane beach. *J. Fluid Mech.* **301**, 251–268.

- BLONDEAUX, P., VITTORI, G. & DE SWART, H. E. 1994 Subharmonic edge wave excitation by waves incident on partially absorbing beaches. In *Sediment Transport Mechanics in Coastal Environments and Rivers* (ed. M. Belorgey, R. D. Rajaona & J. F. A. Sleath), pp. 53–63. World Scientific.
- BOWEN, A. J. 1969 Rip currents, 1: theory. *J. Geophys. Res.* **74**, 5467–5478.
- BOWEN, A. J. & HOLMAN, R. A. 1989 Shear instabilities on the mean longshore current. 1, Theory. *J. Geophys. Res.* **94**, 18023–18030.
- BRUUN, P. 1954 Coast erosion and the development of beach profiles. *Tech. Memo. N. 44*. Beach Erosion Board, U.S. Army Corp Engr., Waterways Expt. Stn, Vicksburg, MS.
- CARRIER, G. F. 1966 Gravity waves on water of variable depth. *J. Fluid Mech.* **24**, 641–659.
- CLOS-ARCEDEC, A. 1962 Etude sur les vues aeriennes, des alluvions littorales d'allure periodique, cordons littoraux et fostons. *Bull. Soc. Fr. Photogramm* **4**, 13–21.
- COLOMBINI, M., SEMINARA, G. & TUBINO M. 1987 Finite-amplitude alternate bars. *J. Fluid Mech.* **181**, 213–232.
- DAVIDSON-ARNOTT, R. G. D. & GREENWOOD, B. 1976 In *Beach and Nearshore Sedimentation* (ed. Soc. Econ. Paleontol. Mineral. Spec. Publ. 24, R. A. Davis & R. L. Ethington), pp. 149–168.
- DEAN, R. G. 1976 Beach erosion: causes, processes and remedial measures. In *CRC Reviews in Environmental Control*, vol. 6, ds 3, pp. 259–269. CRC Press.
- DE SWART, H. E., BLONDEAUX, P. & VITTORI, G. 1995 Edge waves and steady currents near a vertical cliff. In *Structure and Dynamics of Nonlinear Waves in Fluids* (ed. K. Kirchgässner & A. Mielke), pp. 191–200. World Scientific.
- DYER, K. R. 1986 *Estuarine and Coastal Sediment Dynamics*. John Wiley & Sons.
- ECKART, C. 1951 Surface waves on water of variable depth. *Wave Rep.* 100. Scripps Inst. of Oceanogr., Univ. of California, La Jolla.
- FREDSØE, J. 1974 On the developments of dunes on erodible channels. *J. Fluid Mech.* **64**, 1–16.
- FREDSØE, J. & DEIGAARD R. 1992 *Mechanics of Coastal Sediment Transport*. World Scientific.
- GUZA, R. T. & DAVIS, R. E. 1974 Excitation of edge waves by waves incident on a beach. *J. Geophys. Res.* **79** 9, 1285–1291.
- HINO, M. 1974 Theory of formation of rip current and cuspidal coast. In *Proc. 14th Coastal Engng. Conf. Copenhagen*, pp. 901–919. ASCE.
- HOLLAND, K. T. & HOLMAN, R. A. 1996 Field observations of beach cusps and swash motions. *Mar. Geol.* **134**, 77–93.
- HOLMAN, R. A. & BOWEN, A. J. 1982 Bars, bumps and holes: models for the generation of complex beach topography. *J. Geophys. Res.* **87**, C3, 457–468.
- HOM-MA, M. & SONU, C. 1963 Rhythmic pattern of longshore bars related to sediment characteristics. In *8th Coastal Engng. Conf., Mexico City, November 1962*, pp. 248–278.
- HOWD, P. A. & BIRKEMEIER, W. A. 1987 Beach and nearshore survey data: 1981–1984 CERC Field Research Facility. *Tech. Rep.* CERC-87-9. Coastal Engng. Res. Center, USAE Waterways Experiment Station, Vicksburg, MS.
- HULSCHER, S. J., DE SWART, H. E. & DE VRIEND, H. J. 1993 The generation of offshore tidal sand banks and sand waves. *Cont. Shelf Res.* **13**, 1183–1204.
- INMAN, D. L. & BAGNOLD, R. A. 1963 Littoral processes. In *The Sea: Ideas and Observations*, vol. 3. Interscience.
- INMAN D. L., ELWANY, M. H. S. & JENKINS, S. A. 1993 Shorerise and bar-berm profiles on ocean beaches. *J. Geophys. Res.* **98**, C10, 18181–18199.
- INMAN, D. L. & GUZA, R. T. 1982 The origin of swash cusps on beaches. *Mar. Geol.* **49**, 133–148.
- KOMAR, P. D. 1971 The mechanics of sand transport on beaches. *J. Geophys. Res.* **76**, 713–721.
- KOMAR, P. D. 1977 Beach sand transport: distribution and total drift. *Proc. ASCE J. Waterways, Harbours and Coastal Engng.* **4**, 225–239.
- KOMAR, P. D. 1998 *Beach Processes and Sedimentation*, 2nd edn. Prentice-Hall.
- LEE, G. & BIRKEMEIER, W. A. 1993 Beach and nearshore survey data: 1985–1991 CERC Field Research Facility. *Tech. Rep.* CERC 93-3. Coastal Engng. Res. Center, USAE Waterways experimental Station, Vicksburg, MS.
- LIPPMAN, T. C., HOLMAN, R. A. & BOWEN, A. J. 1997 Generation of edge waves in shallow water. *J. Geophys. Res.* **102**, 8663–8679.
- MEI, C. C. 1989 *The Applied Dynamics of Ocean Surface Waves*. World Scientific.

- MINZONI, A. A. & WHITHAM, G. B. 1977 On the excitation of edge waves on beaches. *J. Fluid Mech.* **79**, 273–287.
- PARKER, G. 1976 On the cause and characteristic scales of meandering and braiding in rivers. *J. Fluid Mech.* **76**, 457–480.
- PRUSZAK, Z., ROZYNSKY, G. & ZEIDLER, R. B. 1997 Statistical properties of multiple bars. *Coastal Engng* **31**, 263–280.
- RIBBERINK, J. S. & AL-SALEM, A. A. 1994 Sediment transport in oscillatory boundary layers in cases of rippled beds and sheet flow. *J. Geophys. Res.* **99**, C6, 12707–12727.
- RICHARDS, K. J. 1980 The formation of ripples and dunes on an erodible bed. *J. Fluid Mech.* **99**, 597–690.
- SCHIELEN, R., DOELMAN, A. & DE SWART, H. E. 1993 On the nonlinear dynamics of free bars in straight channels. *J. Fluid Mech.* **252**, 325–356.
- SEYMOUR, R. J. & AUBREY, D. G. 1985 Rhythmic beach cusps formation: a conceptual synthesis. *Mar. Geol.* **65**, 289–304.
- SUMER, M. & BAKIOGLU, M. 1984 On the formation of ripples on an erodible bed. *J. Fluid Mech.* **144**, 177–190.
- VAN RIJN, L. C. 1990 Sediment transport in combined waves and currents. In *Proc. Euromech 262: Sand Transport in Rivers, Estuaries and the Sea* (ed. R. Soulsby, & R. Bettess), pp. 3–15. Balkema.
- VAN RIJN, L. C. 1993 *Principles of Sediment Transport in Rivers, Estuaries and Coastal Seas*. Aqua Publ.
- VITTORI, G. & BLONDEAUX, P. 1992 Sand ripples under sea waves. Part 3. Brick-pattern ripple formation. *J. Fluid Mech.* **239**, 23–45.
- WERNER, B. T. & FINK, T. M. 1993 Beach cusps as self-organized patterns. *Science* **260**, 968–971.